Supporting Information for "Unimolecular Reactions of Peroxy Radicals Formed in the Oxidation of α-pinene and β-pinene by Hydroxyl Radicals"

Lu Xu[†], Kristian H. Møller[§], John D. Crounse[†], Rasmus V. Otkjær[§], Henrik G. Kjaergaard[§], Paul O. Wennberg[†,⊥]

[†]Division of Geological and Planetary Sciences, California Institute of Technology, Pasadena, California 91125, United States

[§]Department of Chemistry, University of Copenhagen, Universitetsparken 5, DK-2100, Copenhagen Ø, Denmark

[⊥]Division of Engineering and Applied Science, California Institute of Technology, Pasadena, California 91125, United States

Table of Contents

S1. Peak identification of α-pinene and β-pinene hydroxy nitrates

The structural assignment of α-pinene and β-pinene hydroxy nitrate isomers is achieved by the collection of several chromatograms. Firstly, the ring-opened HNs (i.e., 3-OH,8-ONO_2 for α-pinene and 1-OH,8-ONO_2 for β-pinene) are identified by adding O_3 to the chamber after photooxidation. The ring-opened HNs are unsaturated and thus react with O_3 while the ring-retained HN isomers are saturated and will not do so. After the photooxidation ceases, we remove the chamber content through a cold trap (i.e., 6.5 m ¼ inch PFA tubing submerged in -60°C isopropanol + liquid nitrogen bath). The oxidation products are trapped, but volatile compounds including precursor hydrocarbon, NO, NO_2 are not. Then, we remove the tubing from the trap and use a flow of zero air to send the trapped analytes back to chamber. 2-4 ppmv O_3 is added to chamber using an O_3 generator. We also inject approximately 90 ppmv cyclohexane, which serves as an OH scavenger. As shown in Figure S 1, the last peaks for both monoterpenes disappeared after O_3 addition, indicating that they are the ring-opened HNs.

The HNs with the –ONO_2 group on the less-substituted carbon (2-OH,3-ONO_2 for α-pinene and 2-OH,1-ONO_2 for β-pinene) are identified from NO_3 radical oxidation experiments. This approach is based on the assumption that NO_3 radicals react with alkenes by primarily adding to the less-substituted olefinic carbon[1]. Oxygen adds to the alkyl radical and these RO_2 react with other RO_2 to produce hydroxy nitrate (Scheme S 3). We perform NO_3 oxidation experiments by mixing ~200ppb NO and ~300ppb O_3 in an 800 L chamber, waiting for 1 hr to produce NO_3 and N_2O_5, and injecting about 80 ppbv α-pinene or β-pinene. The chromatograms of HNs from NO_3 oxidation experiments are shown in Figure S 2. For both α-pinene and β-pinene, only one peak is resolved from NO_3 oxidation experiments and the retention time of this peak matches that of the first in OH oxidation experiments.

The remaining peak in the OH oxidation is identified based on previous finding that the retention order for HNs with similar structures is generally tertiary –OH, secondary –OH, and then primary –OH for the same GC column [2]. This observation has a plausible rational as the primary –OH likely has stronger interaction with GC column than secondary or tertiary OH due to less shielding effects. Thus, the second peak in the α-pinene chromatogram is assigned to 3-OH,2-ONO_2, which has a secondary –OH and elutes later than 2-OH,3-ONO_2 with a tertiary –OH. Similarly, the second peak in the β-pinene chromatogram is assigned to 1-OH,2-ONO_2. We further

verify the structural assignment of HN peaks by comparing the chromatograms between α-pinene and β-pinene using the same GC temperature profile (Figure S 3). α-pinene 3-OH,2-ONO_2 elutes between β-pinene 2-OH,1-ONO_2 and 1-OH,2-ONO_2, which is consistent with the rule of thumb described above. The ring-opened HNs elute later than ring-retained HNs because the ring-opened HNs are more elongated.

Each peak in the 1 m chromatogram represents one structural isomer of HNs, but each peak includes more than one diastereoisomer. Theoretically, there are ten diastereoisomers for α-pinene HNs and five for β-pinene HNs, as shown in Scheme S 2. These diasteroisomers can be better separated using a 5 m Restek RTX-1701 GC column (Figure S 10). For example, all four ring-retained β-pinene HNs are separated with a 5 m GC column. The first peak in α-pinene HNs with 1 m GC is separated into two peaks with 5 m GC. Not all ten diastereoisomers are separated for α-pinene HNs, likely due to some diastereoisomers co-eluting. Despite of improved separation, significant transmission loss of the ring-opened HN (i.e., the last peak) is observed in the 5 m GC. Because the key information for determination of the RO_2 isomerization rate is the separation of ring-opened HNs from ring-retained HNs (e.g., 3-OH,8-ONO_2 vs. 3-OH,2-ONO_2+2-OH,3-ONO_2 in the α-pinene system), all of which are adequately separately using 1 m GC, we focus our analysis on the data produced using the 1 m GC column.

For α-pinene, the abundance of ring-retained HNs and ring-opened HN is determined by summing up the chromatogram signal from 700-1050 s and 1050-1350 s, respectively, after subtracting the sample background. For β-pinene, the second peak has an apparent tailing, which interference with the signal of the third peak. We apply Lorentzian function to represent the tailing of the second peak (i.e., 1150-1800 s), extrapolate the fitting, and subtract the fitted function from the 1800-2500 s data (Figure S 11). The abundance of the ring-opened HN (i.e., the third peak) is determined by summing up the corrected signal between 1800 and 2500 s. The abundance of the ring-retained HNs is determined by summing up the signal between 500 s and 2500 s and then subtracting the abundance of the third peak. The uncertainty in the isomer abundance mainly arises from the extrapolation of the tail of the second peak. To characterize the uncertainty in ring-opened HN/ring-retained HNs ratio caused by the extrapolation, we applied bootstrap analysis. In the analysis, we randomly select the start point (within range 1100-1200 s) and stop point (within range 1700-1800 s) of the Lorentzian fit and then calculate the isomer ratio of each bootstrap trial.

The 25th and 75th percentiles of 1000 trials are used to represent the uncertainty of isomer ratio, which is within 12% of the median value.

To further separate the structural isomers of the α-pinene ring-retained HNs, we use a deconvolution algorithm[3] to analyze the 1 m chromatograms. Four equal-width Gaussian functions are fitted to the chromatogram signal from 700 to 1050 s, with two peaks representing the 3-OH,2-ONO_2 and the other two peaks representing 2-OH,3-ONO_2. A representative chromatogram fitting is shown in Figure S 12. For β-pinene, the four ring-retained HNs are clearly separated with 5 m GC, so we use the 5 m GC to obtain the relative abundance of ring-retained HNs. For the diastereoisomer pair of β-pinene 1-OH,2-ONO_2, the abundance of *syn* isomer is roughly 4 times higher than that of *anti* isomer, assuming the same sensitivity towards both diastereoisomers. This observation suggests that O_2 preferentially adds to 1-OH,R• from the less sterically hindered side without the two methyl substituents on the four-membered ring.

The GC transmission efficiency of an analyte is determined by the ratio of total chromatogram signal to the amount of analyte trapped in the GC (i.e., product of signal during direct sampling from the bag and trapping time). In the experiments with >1000 ppbv NO when all hydroxy nitrate isomers are produced, the GC transmission efficiencies of α-pinene and β-pinene hydroxy nitrates are 79±4% and 99±5%, respectively. In the experiments with no additional NO injection when only ring-retained hydroxy nitrates are produced, the GC transmission efficiencies of α-pinene and β-pinene hydroxy nitrates are 86±5% and 100%, respectively. The similar transmission efficiencies between experiments with different NO concentrations suggest that the transmission efficiency is isomer-independent within each monoterpene.

Different GC temperature profiles are used, depending on monoterpenes and column length.

- α-pinene and 1m GC: -20°C, + 20°C min^{-1} until 50°C, then +3°C min^{-1} until 120°C, hold 3 min.
- α-pinene and 5m GC: 30°C, + 20°C min^{-1} until 80°C, hold 100 min, then +20°C min^{-1} until 150°C, hold 10 min.
- β-pinene and 1m GC: -20°C, + 20°C min^{-1} until 80°C, hold 25 min, then +10°C min^{-1} until 130°C, hold 15 min.
- β-pinene and 5m GC: 30°C, + 20°C min^{-1} until 110°C, hold 25 min, then +20°C min^{-1} until 150°C, hold 4 min.

S2. Relationship between the (ring-opened HN):(ring-retained HNs) ratio and RO_2 lifetimes

We utilize the ratio of the ring-opened HN relative to that of the ring-retained HNs to probe the unimolecular reactions of ring-opened RO_2. Below, we use a mathematical derivation to illustrate the relationship between the (ring-opened HN):(ring-retained HNs) ratio and RO_2 bimolecular and unimolecular lifetimes. We use α-pinene 2-OH,3-ONO_2 as an example of ring-retained HN. α-pinene 3-OH,8-ONO_2 is the ring-opened HN. In the absence of secondary chemistry, the production rates of 3-OH,8-ONO_2 and 2-OH,3-ONO_2 at time t_i are defined in Eqn. S(1) and S(2).

$$\frac{d[\text{3-OH,8-ONO}_2]}{dt} = BR_{\text{3-OH,8-ONO2}} \times k_{RO_2+NO}[\text{3-OH,8-RO}_2][NO] \quad \text{Eqn. S(1)}$$

$$\frac{d[\text{2-OH,3-ONO}_2]}{dt} = BR_{\text{2-OH,3-ONO2}} \times k_{RO_2+NO}[\text{2-OH,3-RO}_2][NO] \quad \text{Eqn. S(2)}$$

where the $BR_{3\text{-OH,8-ONO2}}$ and $BR_{2\text{-OH,3-ONO2}}$ are the branching ratio to produce organic nitrate from RO_2+NO.

The time-rate-of-change of the two RO_2 at time t_i, in the absence of RO_2 + RO_2 chemistry (reasonable assumption given the low VOC concentration in this study) can be described by Eqn. S(3) and S(4)

$$\frac{d[\text{3-OH,8-RO}_2]}{dt} = Y_{\text{3-OH,8-RO}_2} \times k_{\alpha p+OH}[\alpha\text{-pinene}][OH] - k_{RO_2+NO}[\text{3-OH,8-RO}_2][NO] - k_{RO_2+HO_2}[\text{3-OH,8-RO}_2][HO_2] - k_{unimolecular}[\text{3-OH,8-RO}_2] \quad \text{Eqn. S(3)}$$

$$\frac{d[\text{2-OH,3-RO}_2]}{dt} = Y_{\text{2-OH,3-RO}_2} \times k_{\alpha p+OH}[\alpha\text{-pinene}][OH] - k_{RO_2+NO}[\text{2-OH,3-RO}_2][NO] - k_{RO_2+HO_2}[\text{2-OH,3-RO}_2][HO_2] \quad \text{Eqn. S(4)}$$

where, $Y_{3\text{-OH,8-RO2}}$ and $Y_{2\text{-OH,3-RO2}}$ are the yields of corresponding RO_2, $k_{\alpha p+OH}$, k_{RO2+NO}, $k_{RO2+HO2}$, $k_{unimolecular}$ are the rate coefficients for α-pinene+OH, RO_2+NO, RO_2+HO_2, and RO_2 unimolecular reactions, respectively. We assume that k_{RO2+NO} and $k_{RO2+HO2}$ are isomer independent and all the branching ratios and RO_2 yields are constants.

The steady state concentration of RO_2 can be expressed by:

$$[\text{3-OH,8-RO}_2] = \frac{Y_{\text{3-OH,8-RO}_2} \times k_{\alpha p+OH}[\alpha\text{-pinene}][OH]}{k_{RO_2+NO}[NO] + k_{RO_2+HO_2}[HO_2] + k_{unimolecular}} \quad \text{Eqn. S(5)}$$

$$[\text{2-OH,3-RO}_2] = \frac{Y_{\text{2-OH,3-RO}_2} \times k_{\alpha p+OH}[\alpha\text{-pinene}][OH]}{k_{RO_2+NO}[NO] + k_{RO_2+HO_2}[HO_2]} \quad \text{Eqn. S(6)}$$

Substituting Eqn. S(5) and S(6) into the ratio between Eqn. S(1) and S(2), we get

$$\frac{\frac{d[\text{3-OH,8-ONO}_2]}{dt}}{\frac{d[\text{2-OH,3-ONO}_2]}{dt}} = \frac{BR_{\text{3-OH,8-ONO2}}}{BR_{\text{2-OH,3-ONO2}}} \times \frac{[\text{3-OH,8-RO}_2]}{[\text{2-OH,3-RO}_2]}$$

$$= \frac{BR_{\text{3-OH,8-ONO2}}}{BR_{\text{2-OH,3-ONO2}}} \times \frac{Y_{\text{3-OH,8-RO}_2}}{Y_{\text{2-OH,3-RO}_2}} \times \frac{k_{RO_2+NO}[NO]+k_{RO_2+HO_2}[HO_2]}{k_{RO_2+NO}[NO]+k_{RO_2+HO_2}[HO_2]+k_{\text{unimolecular}}} \quad \text{Eqn. S(7)}$$

The RO_2 unimolecular lifetime $\tau_{\text{unimolecular}}$ (defined in Eqn. S(8)) is a constant, but the instantaneous RO_2 bimolecular lifetime $\tau_{\text{bimolecular,ins}}$ (defined in Eqn. S(9)) changes over the duration of experiments due to varying $[HO_2]$ and $[NO]$.

$$\tau_{\text{unimolecular}} = \frac{1}{k_{\text{unimolecular}}} \quad \text{Eqn. S(8)}$$

$$\tau_{\text{bimolecular,ins}} = \frac{1}{k_{RO_2+NO}[NO]_{t_i} + k_{RO_2+HO_2}[HO_2]_{t_i}} \quad \text{Eqn. S(9)}$$

Substitute Eqn. S(8) and S(9) into Eqn. S(7), we get

$$\frac{\frac{d[\text{3-OH,8-ONO}_2]}{dt}}{\frac{d[\text{2-OH,3-ONO}_2]}{dt}} = \frac{BR_{\text{3-OH,8-ONO2}}}{BR_{\text{2-OH,3-ONO2}}} \times \frac{Y_{\text{3-OH,8-RO}_2}}{Y_{\text{2-OH,3-RO}_2}} \times \frac{\frac{1}{\tau_{\text{bimolecular,ins}}}}{\frac{1}{\tau_{\text{bimolecular,ins}}} + \frac{1}{\tau_{\text{unimolecular}}}}$$

$$= \frac{BR_{\text{3-OH,8-ONO2}}}{BR_{\text{2-OH,3-ONO2}}} \times \frac{Y_{\text{3-OH,8-RO}_2}}{Y_{\text{2-OH,3-RO}_2}} \times \frac{\tau_{\text{unimolecular}}}{\tau_{\text{unimolecular}}+\tau_{\text{bimolecular,ins}}} \quad \text{Eqn. S(10)}$$

By integrating Eqn. S(10) over the duration of the experiment, we get

$$\frac{\Delta[\text{3-OH,8-ONO}_2]}{\Delta[\text{2-OH,3-ONO}_2]} = \frac{BR_{\text{3-OH,8-ONO}_2}}{BR_{\text{2-OH,3-ONO}_2}} \times \frac{Y_{\text{3-OH,8-RO}_2}}{Y_{\text{2-OH,3-RO}_2}} \times \frac{\tau_{\text{unimolecular}}}{\tau_{\text{unimolecular}}+\tau_{\text{bimolecular}}} \quad \text{Eqn. S(11)}$$

where $\tau_{\text{bimolecular}}$ represents the average RO_2 bimolecular lifetime over the duration of the experiment. Thus, by plotting $\frac{\Delta[\text{3-OH,8-ONO}_2]}{\Delta[\text{2-OH,3-ONO}_2]}$ as a function of $\tau_{\text{bimolecular}}$, we can calculate $\tau_{\text{unimolecular}}$, which is $1/k_{\text{unimolecular}}$. In the actual analysis, the sum of two structural isomers of the ring-retained HNs (2-OH,3-ONO_2 and 3-OH,2-ONO_2) is used.

To calculate $\tau_{\text{bimolecular}}$, we estimate the concentrations of NO and HO_2 from modified Master Chemical Mechanims (MCM)[4]. The major modifications we make are (1) updating the nitrate branching ratio based on measurements (Section S6) and (2) updating the ring-opening fraction of activated alkyl radical based on RO-CCSD(T)-F12a/VDZ-F12//ωB97X-D/aug-cc-

pVTZ calculation (Section S5.3). We also include the unimolecular reactions of ring-opened RO_2. Because a myriad of products is produced from the unimolecular reactions, we assume the unimolecular reactions of ring-opened RO_2 produce a generic RO_2 in the model. As this assumption conserves the RO_2 concentration, unimolecular reactions have little effect on the NO and HO_2 concentrations.

The measured concentrations of NO, hydrocarbon (α-pinene or β-pinene), and CH_3ONO are used as initial concentrations in MCM. The measured spectral radiance of the chamber light is input in MCM, but is adjusted until the modeled hydrocarbon decay agrees with measurements. The modeled NO and HO_2 concentrations over the course of photooxidation are used to calculate $\tau_{bimolecular,ins}$. As the NO and HO_2 concentrations change over time, we calculate an average $\tau_{bimolecular}$ by weighting the $\tau_{bimolecular,ins}$ by the instantaneous α-pinene consumption amount in each simulation time step. The uncertainty in $\tau_{bimolecular}$ is represented by the range of $\tau_{bimolecular,ins}$ from the beginning to the end of photooxidation. As shown in Figure 2, the uncertainty increases with longer $\tau_{bimolecular}$.

For experiments with no initial NO injection (i.e., Experiments 6 and 13 in Table S 1), we estimate the concentrations of NO and HO_2 by following the procedures in Crounse et al. and Teng et al. [5-6] In brief, the HO_2 concentration is calculated from the measured production rate of H_2O_2 and rate coefficient for the HO_2+HO_2. The NO concentration is inferred from HO_2 concentration and the measured production rates of hydroxy nitrate and hydroxy hydroperoxides. The calculated $\tau_{bimolecular}$ from this method are 3.8 s and 8.9 s for Experiments 6 and 13, respectively, which agree well with the values estimated using MCM, which are 5.7 s and 9.5 s, respectively.

We also calculate $\tau_{bimolecular}$ using the default nitrate branching ratio in MCM. Figure S 13 compares the $\tau_{bimolecular}$ calculated by using updated and default nitrate branching ratio. The difference is negligible. This is mainly because NO concentration is close to its initial concentration, as a result of small OH exposure in the experiments.

S3. Computational approach

S3.1 Dipole moments and polarizabilities

Dipole moments and polarizabilities are calculated for (1) the 15 different hydroxy nitrates formed by addition of OH, O_2 and subsequently NO to α-pinene and β-pinene (Table S 2); (2) the 15 different hydroxy hydroperoxides formed by addition of OH, O_2 and reaction with HO_2 to α-pinene and β-pinene (Table S 3); (3) glycolaldehyde used as a calibration reference and endoperoxide ketoaldehyde (P2 in Scheme 3) formed later in the α-pinene oxidation (Table S 4).

The dipole moments and polarizabilities are calculated using an approach previously employed [7-9]. Briefly, the structures are drawn and a conformational sampling is carried out using MMFF in Spartan '14 [10-16]. All resulting structures are optimized at the B3LYP/6-31+G(d) level in Gaussian 16, rev. A.03 [17-22] with default convergence criteria and integration grid. All unique structures within 15 kJ/mol in electronic energy of the lowest-energy conformer are further optimized using B3LYP/cc-pVTZ [23]. The average dipole moment of each structure is calculated as a Boltzmann weighted average of the conformers at 298 K. The polarizability is calculated only for the lowest-energy conformer of each isomer, as it varies by less than 3% between conformers of the same compound. The calculated CIMS sensitivities of a few test compounds using the augmented aug-cc-pVTZ basis set change by less than 4 % compared to the values obtained using cc-pVTZ, see Table S 5.

S5.2 The rate coefficients of unimolecular reactions

The rate coefficients of the unimolecular reactions of the peroxy radicals are calculated using the approach by Møller et al. [24] For the reactant and transition state, a conformational sampling is carried out in Spartan'14 or '16 using MMFF with a neutral charge enforced on the radical center [10-16, 25]. For the reactant, the input is a geometry simply drawn. For the transition state, the conformational sampling is preceded by an optimization using B3LYP/6-31+G(d) in Gaussian 16, rev. A.03, which is then used as input for the conformer search [17-22]. Furthermore, during the conformational sampling of the transition state, three bond lengths are constrained to the values from the optimized TS: For the H-shifts, the peroxy O-O length, the O···H length and the H···C (or H···O) length and for the endoperoxide formations, the peroxy O-O length, the length of the O···C bond forming and the length of the C-C bond going from a double to a single bond [24]. The structures resulting from the conformer searches are optimized using B3LYP/6-31+G(d) in

Gaussian 16. For the transition states, the free transition state optimization is preceded by a constrained optimization using the same constraints as for the conformational sampling. Conformers within $1 \cdot 10^{-5}$ hartree and $1.5 \cdot 10^{-2}$ D in energy and dipole moment, respectively, of each other are identified as duplicates and only one is kept.[24] All unique conformers with electronic energies within 2 kcal/mol of the lowest-energy conformer are further optimized at the ωB97X-D/aug-cc-pVTZ level of theory [23, 26-27]. In Møller et al., a cut-off based on electronic energy at this level was found to be suitable.

For the lowest-energy conformer (based on electronic plus zero-point vibrational energy (ZPVE)) at this level, an RO-CCSD(T)-F12a/VDZ-F12//ωB97X-D/aug-cc-pVTZ (abbreviated F12) single-point calculation is done using Molpro 2012 [28-34]. This has not been done for H-shifts that abstract from an OH group, and thus the rate coefficients for these are expected to have a slightly higher uncertainty. All F12 calculations have T1 values lower than 0.025, which is well below the value of 0.04 generally accepted for open-shell systems[35-37]. For the reactions of A1, Gaussian 09, rev. D.01 was used instead of Gaussian 16, but the approach was otherwise identical. For both the calculations in Gaussian 09 and 16, the default convergence criteria were used along with the ultrafine integration grid, which is the default in Gaussian 16. In Møller et al., it was found that the default optimization convergence criteria in Gaussian 09 yielded rate coefficients within 1 % of those obtained using "opt=verytight".

From the B3LYP/6-31+G(d) optimized TS structure of the conformer corresponding to the lowest-energy conformer (based on electronic plus ZPVE) at the ωB97X-D/aug-cc-pVTZ level, an IRC is calculated at the B3LYP/6-31+G(d) level using the "calcall" keyword. The IRC end-points are optimized first using B3LYP/6-31+G(d) and subsequently using ωB97X-D/aug-cc-pVTZ. Finally, an F12 single-point calculation is done. Eckart tunneling coefficients are calculated in MATLAB R2016b using barrier heights with F12 electronic energies and ωB97X-D/aug-cc-pVTZ ZPVE and the imaginary frequency of the TS calculated using ωB97X-D/aug-cc-pVTZ [38-39].

Reaction rate coefficients, k, are calculated using multi-conformer transition state theory (MC-TST) [24, 40-42]:

$$k = \kappa \frac{k_B T}{h} \cdot \frac{\sum_i^{All\ TS\ conf.} \exp\left(-\frac{\Delta E_i}{k_B T}\right) Q_{TS_i}}{\sum_j^{All\ R\ conf.} \exp\left(-\frac{\Delta E_j}{k_B T}\right) Q_{TS_j}} \cdot \exp\left(-\frac{E_{TS} - E_R}{k_B T}\right) \quad \text{Eqn. S(12)}$$

where k_B is the Boltzmann constant, T is the absolute temperature, h is Planck's constant, the sums are over all transition state and reactant conformers, respectively and sum their partition functions (Q) Boltzmann weighted by their energy calculated relative to the lowest-energy conformer. The final term has the energy difference between the lowest-energy TS and reactant conformers, the barrier height. The barrier heights are calculated using F12 electronic energies with ωB97X-D/aug-cc-pVTZ ZPVE and ωB97X-D/aug-cc-pVTZ is used for the partition functions and relative energy between conformers. The partition functions are calculated using the harmonic oscillator rigid rotor approximation. All reaction rate coefficients are calculated at 298.15 K. Rate coefficients calculated at this level are given in Table S 6 and Table S 7.

Rate coefficients calculated similarly, but using ωB97X-D/aug-cc-pVTZ for all values including the electronic energy are given in Table S 8 and Table S 9. The rate coefficients of three unimolecular channels (i.e., 1,5 H-shift, 1,6 H-shift, and 6-membered endoperoxide formation) of A1 using ωB97X-D/aug-cc-pVTZ were reported in Berndt et al. [43]

As an approach for eliminating slow reactions, MC-TST reaction rate coefficients were calculated following the B3LYP/6-31+G(d) calculations for all reactions (Table S 10 and Table S 11). For these reactions, tunneling was estimated from the barrier height (energy difference between lowest-energy reactant and TS conformers) and assuming a thermoneutral reaction (i.e. a symmetrical barrier) [44]. The Eckart tunneling coefficient is thus calculated with same forward and reverse barriers, which are equal to the reaction barrier and the imaginary frequency of the lowest-energy (E_e+ZPVE) conformer at the B3LYP/6-31+G(d) level. Compared to the more formally correct approach of using the IRC end-points for the tunneling barriers, this is expected to represent an upper limit for the Eckart tunneling correction (with a given imaginary frequency) [24]. Firstly, the reaction barrier is the upper limit for the forward Eckart barrier and likely the IRC connects to a higher-energy reactant conformer [24]. Secondly, the peroxy radical H-shift reactions are generally energetically uphill, which means that the reverse IRC barrier is usually lower than the forward. For the unimolecular reactions of B5 (the ring-opened β-pinene hydroxy peroxy radical), we show that the Eckart tunneling coefficients calculated using this approach do indeed represent upper limits for the B3LYP Eckart tunneling coefficient, see Table S 12. The use of upper limit tunneling coefficients for the MC-TST B3LYP reaction rate coefficients allows to more confidently eliminate slow reactions at this level. Reactions with rate coefficients below $5 \cdot 10^{-3}$ s^{-1} were not

considered at a higher level. However, for a few reactions with rate coefficient below this value, higher-level reaction rate coefficients were calculated to validate the value of the cut-off.

S5.3 Calculations on the ring-opening fraction of hydroxy alkyl radicals

Conformational sampling and subsequent computational steps were done as described in the approach by Møller et al. (see above) [24] using Gaussian 09 for the DFT calculations. For the RRKM simulations, the electronic energy of the species important for the simulation (the free reactants, the hydroxy alkyl radicals and the ring-opening TS) are calculated using RO-CCSD(T)-F12a/VDZ-F12//ωB97X-D/aug-cc-pVTZ (abbreviated F12) while all other values are calculated using ωB97X-D/aug-cc-pVTZ. For reference, the canonical (for the species without excess energy) MC-TST reaction rate coefficients for the ring-opening reactions are also calculated using the approach described above (but these values are not used in the simulation). The canonical MC-TST reaction rate coefficients do not include a tunneling correction due to the large mass being transferred (tunneling coefficient estimated to be less than a factor of 2). The Eckart tunneling correction is used in the simulations.

RRKM modelling is done using the Master Equation Solver for Multi-Energy well Reactions (MESMER) for the lowest-energy conformers (MESMER uses only a single conformer)[45]. For the simulations, the following parameters are used:

- k(α-pinene + OH, 300 K) = $6.08 \cdot 10^{-11}$ cm^{-3} molecule^{-1} s^{-1} , [46]
- k(β-pinene + OH, 300 K) = $7.72 \cdot 10^{-11}$ cm^{-3} molecule^{-1} s^{-1} , [46]
- [OH] = $1 \cdot 10^{6}$ molecules cm^{-3} corresponding to the estimated global average value.
- k(R·+O_2) = $14 \cdot 10^{-12}$ cm^{-3} molecule^{-1} s^{-1} [47]. This is the value for cyclohexanyl + O_2 and corresponds to a pseudo-first order rate coefficient of $7.2 \cdot 10^{7}$ s^{-1}. The exact rate of this addition is not important for the simulation, as long as it is significantly faster than the rate of ring-opening for the thermalized radicals (10^2-10^3 s^{-1}, see Table S 15) and slower than the excess energy reaction (~10^{10} s^{-1}) [48].
- Exponential energy decay with energy transfer per collision (ΔE_{down}) = 225 cm^{-1}. This value is based on values for similar simulations with N_2 as the bath gas [49-50].
- Lennard-Jones parameters for the pinene-derived species: σ = 6.5 Å, ε/k_b = 600 [50].
- Bath gas = N_2 (σ = 3.919 Å, ε/k_b = 91.85) [51]
- P = 760 Torr, T = 298.15 K

- Grain size = 100 cm^{-1} and energy grain span above the highest stationary point = $50k_BT$.

The system being modelled is illustrated for β-pinene in Figure S 14 for exemplification. As can be seen, the hydroxy alkyl radical is formed with almost 30 kcal/mol excess energy and the barrier for ring-opening is about 13 kcal/mol. As shown in Table S 15, the energetics are very similar for all three systems. As expected from the comparable energetics of the three systems, the calculated amount modelled to ring open is very similar for all three at around 30-50 % (Table S 15). The difference between α-pinene and β-pinene is within the uncertainty of the modelling. Very similar results are obtained when all values are calculated using ωB97X-D/aug-cc-pVTZ (Table S 16), but with slightly higher barriers leading to slightly lower yields of the ring-opened product.

To assess the sensitivity of the model, the analysis was redone for the systems where the barrier for ring-opening had either been decreased or increased by 1 kcal/mol. As shown in Table S 17, this roughly changes the fraction ring-opening by a factor of two in either direction. We also test the sensitivity of the model towards the energy being transferred per collision (ΔE_{down}), as shown in Table S 18. The results in the table confirm that the ring-opening is driven by the excess energy in the hydroxy alkyl radical, as decreasing the energy transfer per collision increases the yield of ring-opened product and vice versa.

S4. Kinetic box model to simulate the relationship between the (ring-opened HN):(ring-retained HNs) ratio and RO_2 lifetimes

To obtain the distribution of HN isomers under certain $\tau_{bimolecular}$, we solve the time-dependent set of ordinary differential equations (ODEs) for the following systems, which include the oxidation reactions of α-pinene depicted in Scheme 1.

$$\frac{d[\alpha\text{-pinene}]}{dt} = -k_{\alpha p+OH} \times [\alpha\text{-pinene}] \times [OH]$$

$$\frac{d[\text{2-OH,3-RO}_2]}{dt} = Y_{\text{2-OH,3-RO}_2} \times k_{\alpha p+OH}[\alpha\text{-pinene}] \times [OH] - k_{RO_2+NO}[\text{2-OH,3-RO}_2] \times [NO]$$

$$\frac{d[\text{3-OH,2-RO}_2]}{dt} = Y_{\text{3-OH,2-RO}_2} \times k_{\alpha p+OH}[\alpha\text{-pinene}] \times [OH] - k_{RO_2+NO}[\text{3-OH,2-RO}_2] \times [NO]$$

$$\frac{d[\text{3-OH,8-RO}_2]}{dt} = Y_{\text{3-OH,8-RO}_2} \times k_{\alpha p+OH}[\alpha\text{-pinene}] \times [OH] - k_{RO_2+NO}[\text{3-OH,8-RO}_2] \times [NO] - k_{unimolecular}[\text{3-OH,8-RO}_2]$$

$$\frac{d[\text{2-OH,3-ONO}_2]}{dt} = BR_{\text{2-OH,3-ONO}_2} \times k_{RO_2+NO}[\text{2-OH,3-RO}_2] \times [NO]$$

$$\frac{d[\text{3-OH,2-ONO}_2]}{dt} = BR_{\text{3-OH,2-ONO}_2} \times k_{RO_2+NO}[\text{3-OH,2-RO}_2] \times [NO]$$

$$\frac{d[\text{3-OH,8-ONO}_2]}{dt} = BR_{\text{3-OH,8-ONO}_2} \times k_{RO_2+NO}[\text{3-OH,8-RO}_2] \times [NO]$$

The symbols have the same meaning as those in section S2. To achieve the same OH exposure as experiments, we assume a constant OH concentration (2×10^6 molec cm^{-3}) and interval of integration (1000 s). Our procedure to obtain the optimized $k_{unimolecular}$ is the following. First, by solving the set of ODEs under fixed NO concentration and $k_{unimolecular}$, we obtain the (ring-opened HN):(ring-retained HNs) ratio at fixed $\tau_{bimolecular}$ and $k_{unimolecular}$. Second, under a fixed $k_{unimolecular}$ but varying NO concentration, we obtain the relationship between (ring-opened HN):(ring-retained HNs) ratio and $\tau_{bimolecular}$. Third, we vary $k_{unimolecular}$ to obtain different relationships between (ring-opened HN):(ring-retained HNs) ratio and $\tau_{bimolecular}$. Finally, we compare the simulated relationships under varying $k_{unimolecular}$ with measurements to determine the optimized $k_{unimolecular}$. We determine the upper and lower bounds of the $k_{unimolecular}$ in a way that 80% of the experimental data points are placed on the same side of the simulated curve. The upper and lower bounds are used to calculate the average and the uncertainty range of $k_{unimolecular}$ assuming symmetric uncertainties.

S5. Yields of α-pinene and β-pinene hydroxy nitrates

We estimate the instrumental sensitivity (c_x) towards HNs based on the ion-molecular collision rate coefficients (k_x). The rate coefficients are calculated from the dipole moment (μ) and polarizability (α) using the empirical approach developed by Su et al. [52]. The μ and α for all 10 α-pinene HN isomers and 5 β-pinene HNs are calculated using Density Function Theory (DFT) B3LYP/cc-pVTZ (Section S3.1) and are listed in Table S 2.

We relate the k_x to c_x by using glycoaldehyde as a calibration reference

$$c_x = \frac{k_x}{k_{glycoaldehyde}} \times c_{glycoaldehyde}$$

where $k_{glycoaldehyde}$ is 2.0×10^{-9} cm^3 $molec^{-1}$ s^{-1} using the empirical approach by Su et al. [52] and $c_{glycoaldehyde}$ is experimentally determined to be 1.5×10^{-4} ncts $pptv^{-1}$ where ncts (normalized counts) is the observed ion count rate divided by the sum of the count rates for $^{13}CF_3O^-$ and $^{13}CF_3O^-\cdot H_2O$.

The signal of an individual HN isomer is calculated by multiplying the total signal of all HNs during direct sampling by the corresponding GC fractional abundances. Isomer-specific sensitivity is applied to convert the signal to mixing ratio. The molar yield of a HN isomer is the change in HN concentration over the consumed parent hydrocarbon. The overall yield of all HN isomers is the summation over all individual isomers. We quantify the overall yields of HN to be 3.3±1.5% and 6.4±2.1% for α-pinene and β-pinene, respectively. The mean value is obtained from the average of five experiments with initial NO concentration above 1000 ppbv. The uncertainty is calculated by propagating the standard deviations of HN yields from five experiments (15% for α-pinene and 6% for β-pinene), the instrumental sensitivity uncertainty (~30%), initial hydrocarbon concentration uncertainty (~10%), secondary loss (~5%), and vapor wall loss (~2%). The secondary loss of HN by reaction with OH [53] is negligible (<5%) because of the low OH exposure in the experiments (roughly 2×10^9 and 1×10^9 molecules cm^{-3} s for α-pinene and β-pinene experiments, respectively). The measured wall loss rate constant for HN is 1×10^{-5} s^{-1}. In 30 min (i.e., the oxidation time in experiments to quantify the hydroxy nitrate yield), 2% of gas-phase hydroxy nitrate is lost to wall. To evaluate the sample loss in the 2 m Teflon sampling line, we increased the sampling flow rate from 1 LPM to 2 LPM. No discernable change in hydroxy nitrate concentration was observed, suggesting negligible loss in sampling line.

We note that the overall yield reported here only accounts for the first generation gas phase HNs. Considering that less than 10 ppbv hydrocarbon is oxidized, the fraction of HNs in the particle phase is expected to be small. According to Eddingsaas et al. [54] who used similar initial α-pinene concentration as our study, the SOA yield is ~5% when OH exposure is ~2×10^9 molec cm^{-3} s. Thus, roughly 3 μg m^{-3} SOA is produced from the oxidation of 10 ppbv α-pinene. Bean et al. reported that when OA concentration is below 40 μg m^{-3}, only 5–10% of α-pinene organic nitrates are expected to partition to the particle phase [55]. Therefore, the effect of gas/particle partitioning on our measured HNs yield is within 10%. To further test the effect of gas/particle partitioning on the gas phase HN yields, we perform experiments with ~300ppbv initial VOC and oxidize ~30ppbv VOC to keep the OH exposure the same as low VOC experiments. The HNs yields are not statistically significant between high and low VOC experiments (3.2±1.5% when Δα-pinene < 10 ppbv vs. 3.4±1.5% when Δα-pinene = ~30ppbv; 6.3±2.1% when Δβ-pinene < 10ppbv vs. 6.9±2.3% when Δβ-pinene = ~30ppbv), suggesting a minor effect of gas/particle partitioning on HNs yield. From the high vs. low VOC experiments, we also find that the gas/particle partitioning has small effect on the distribution of HN isomers (Figure S 15).

In α-pinene short $\tau_{bimolecular}$ experiments, we observe CIMS signals at a number of even masses (Table S 20). If we assume that the compounds appearing at even mass are nitrogen-containing organic compounds and assume that these compounds have the same sensitivity as the average of all α-pinene hydroxy nitrate isomers, we estimate an overall yield of organic nitrates to be 9%. This roughly estimated yield is half of the total nitrates yield quantified by FT-IR in an earlier study (18%±9%) [56]. However, we note that the alkyl nitrates produced from OH abstraction channel are detected by FTIR, but not by CF_3O^- CIMS, which partly contributes to the discrepancy. The uncertainties in instrumental sensitivity also can largely influence the comparison. Following the same analysis as α-pinene, the overall yield of organic nitrates is estimated to be 11% for β-pinene.

S6. Discussion of branching ratios and associated uncertainties in α-pinene oxidation.

The formation pathway of α-pinene HNs and co-products is shown in Scheme S 7. The branching ratio for each reaction step is discussed below. BR in this study is defined as the ratio of the rate constant for a particular product of a reaction to the rate constant for the total set of possible products[57].

1) BR_{OH_add} represents the fraction of α-pinene + OH that proceeds via addition to the double bond. Early theoretical studies estimate that BR_{OH_add} is 90% based on structure-activity relationships [58-59].

2) $BR_{OH\_less\_sub}$ represents the fraction of OH adding onto the less-substituted olefinic carbon. $BR_{OH\_less\_sub}$ is equivalent to BR_{add_C3} in Scheme S 7 and BR_{add_C1} in Scheme S 8. These ratios have not been experimentally constrained. The OH addition branching ratio for 2-methyl 2-butene, which shares a similar substitutions around the C-C double bond with α-pinene, though does not have the rigid constraints of a ring structure, is 69% : 31% as experimentally constrained in Teng et al. [2] However, Peeters et al. suggested that the bicyclic ring structure may affect the substitution effect and hence conjectured the branching ratio as 50% : 50%.

3) $BR_{ring\text{-}open}$ represents the ring-opening fraction of activated alkyl radicals. $BR_{ring\text{-}open}$ has been extensively discussed in the main text. In brief, Peeters et al.[58] and our theoretical calculations (F12 level) suggest $BR_{ring\text{-}open}$ to be 50% and 32%, respectively for 3-OH,2-R• from α-pinene + OH.

4) BR_{RONO2} represents the nitrate branching ratio of RO_2 reaction with NO to form $RONO_2$ (BR_{RONO2} is shown as "BR1-3" in Scheme S 7). An estimate of BR_{RONO2} for each RO_2 isomer can be calculated from the measured yield of corresponding HN isomer and the branching ratios for each step along HN formation pathway. Using 50% as the BR_{add_C2} (from Peeters et al. [58]) and 32% as the $BR_{ring\text{-}open}$ (from our theoretical calculation), we calculate that the BR_{RONO2} is 3.1%, 0.7%, and 10.8% for α-pinene 2-OH,3-RO_2, 3-OH,2-RO_2, and 3-OH,8-RO_2, respectively. Using the same approach, we estimate that the BR_{RONO2} is 15.9%, 10.2%, and 1.7% for β-pinene 2-OH,1-RO_2, 1-OH,2-RO_2, and 1-OH,8-RO_2, respectively. The widely ranging BR_{RONO2} for RO_2 with similar structures is surprising and may indicate errors in the calculated branching ratios. For example, BR_{RONO2} of α-pinene ring-opened peroxy radical, 3-OH,8-RO_2 (10.8%), is six times larger than that of β-pinene ring-opened peroxy radical, 1-OH,8-RO_2 (1.7%).

Considering the large uncertainties in the above branching ratios, we suggest an alternative constraint on them based on measured yield of hydroxy nitrate isomers. We assume that the ring-opened tertiary RO_2 of both α-pinene and β-pinene have the same BR_{RONO2} (denoted as "$BR_{RONO2,ring\text{-}open}$"). This assumption is reasonable as the ring-opened RO_2 of both terpenes share very similar structure (i.e., tertiary RO_2 in the -$C(CH_3)_2OO$ group). Further, we assume that all the β-hydroxy RO_2 have the same BR_{RONO2} (denoted as "$BR_{RONO2,\beta\text{-}OH}$"), following study by Teng et

al.[6] Based on these two assumptions, we can express the yields of six hydroxy nitrate isomers (α-pinene and β-pinene combined) by propagating the branching ratio of each step as shown below,

$$Y_{\alpha\text{-pinene 3-OH,8-ONO2}} = BR_{OH\_add} \times BR_{add\_C3} \times BR_{\alpha\text{-pinene,ring-open}} \times BR_{RONO2,ring\text{-}open}$$

$$Y_{\alpha\text{-pinene 3-OH,2-ONO2}} = BR_{OH\_add} \times BR_{add\_C3} \times (1- BR_{\alpha\text{-pinene,ring-open}}) \times BR_{RONO2,\beta\text{-}OH}$$

$$Y_{\alpha\text{-pinene 2-OH,3-ONO2}} = BR_{OH\_add} \times (1-BR_{add\_C3}) \times BR_{RONO2,\beta\text{-}OH}$$

$$Y_{\beta\text{-pinene 1-OH,8-ONO2}} = BR_{OH\_add} \times BR_{add\_C1} \times BR_{\beta\text{-pinene,ring-open}} \times BR_{RONO2,ring\text{-}open}$$

$$Y_{\beta\text{-pinene 1-OH,2-ONO2}} = BR_{OH\_add} \times BR_{add\_C1} \times (1-BR_{\beta\text{-pinene,ring-open}}) \times BR_{RONO2,\beta\text{-}OH}$$

$$Y_{\beta\text{-pinene 2-OH,1-ONO2}} = BR_{OH\_add} \times (1-BR_{add\_C1}) \times BR_{RONO2,\beta\text{-}OH}$$

BR_{OH_add} is 0.9 as discussed above. BR_{add_C3} and BR_{add_C1} represent the branching ratio of OH adding onto C3 and C1 in α-pinene and β-pinene, respectively. The yield of each hydroxy nitrate isomer is measured in this study. BR_{add_C3}, BR_{add_C1}, $BR_{\alpha\text{-pinene,ring-open}}$, $BR_{\beta\text{-pinene,ring-open}}$, $BR_{RONO2,\beta\text{-}OH}$, and $BR_{RONO2,ring\text{-}open}$ are unknowns. By solving the system of equations (six equations and six unknowns), we find that

$BR_{add\_C3} = 0.83$,

$BR_{add\_C1} = 0.88$,

$BR_{\alpha\text{-pinene,ring-open}} = 0.97$,

$BR_{\beta\text{-pinene,ring-open}} = 0.34$,

$BR_{RONO2,\beta\text{-}OH} = 0.092$,

$BR_{RONO2,ring\text{-}open} = 0.022$.

To evaluate how the assumption on BR_{RONO2} affects the $BR_{ring\text{-}open}$, we extend the approach by implementing different constraints on BR_{RONO2}. For example, we assume that the ratio of BR_{RONO2} for tertiary, secondary, and primary β-hydroxy RO_2 is 1.25: 1: 0.75 as suggested by Wennberg et al.[60]. Now, the system contains eight equations and eight unknowns, as shown below.

$$Y_{\alpha\text{-pinene 3-OH,8-ONO2}} = BR_{OH\_add} \times BR_{add\_C3} \times BR_{\alpha\text{-pinene,ring-open}} \times BR_{RONO2,ring\text{-}open}$$

$$Y_{\alpha\text{-pinene 3-OH,2-ONO2}} = BR_{OH\_add} \times BR_{add\_C3} \times (1- BR_{\alpha\text{-pinene,ring-open}}) \times BR_{RONO2,\beta\text{-}OH,3rd}$$

$$Y_{\alpha\text{-pinene 2-OH,3-ONO2}} = BR_{OH\_add} \times (1-BR_{add\_C3}) \times BR_{RONO2,\beta\text{-}OH,2nd}$$

$Y_{\beta\text{-pinene 1-OH,8-ONO2}} = BR_{OH\_add} \times BR_{add\_C1} \times BR_{\beta\text{-pinene,ring-open}} \times BR_{RONO2,ring\text{-}open}$

$Y_{\beta\text{-pinene 1-OH,2-ONO2}} = BR_{OH\_add} \times BR_{add\_C1} \times (1\text{-}BR_{\beta\text{-pinene,ring-open}}) \times BR_{RONO2,\beta\text{-}OH,3rd}$

$Y_{\beta\text{-pinene 2-OH,1-ONO2}} = BR_{OH\_add} \times (1\text{-}BR_{add\_C1}) \times BR_{RONO2,\beta\text{-}OH,1st}$

$BR_{RONO2,\beta\text{-}OH,1st} = 0.75 \times BR_{RONO2,\beta\text{-}OH,2nd}$

$BR_{RONO2,\beta\text{-}OH,3rd} = 1.25 \times BR_{RONO2,\beta\text{-}OH,2nd}$

where $BR_{RONO2,\beta\text{-}OH,1st}$, $BR_{RONO2,\beta\text{-}OH,2nd}$, $BR_{RONO2,\beta\text{-}OH,3rd}$ represents the BR_{RONO2} for primary, secondary, and tertiary β-hydroxy RO_2, respectively. Other symbols have the same meaning as in previous equations.

By solving the new system of equations, we find that

$BR_{add\_C3} = 0.81$,

$BR_{add\_C1} = 0.82$,

$BR_{\alpha\text{-pinene,ring-open}} = 0.97$,

$BR_{\beta\text{-pinene,ring-open}} = 0.36$,

$BR_{RONO2,ring\text{-}open} = 0.023$,

$BR_{RONO2,\beta\text{-}OH,1st} = 0.061$,

$BR_{RONO2,\beta\text{-}OH,2nd} = 0.082$,

$BR_{RONO2,\beta\text{-}OH,3rd} = 0.10$.

Different assumptions have minor effect on $BR_{ring\text{-}open}$. More importantly, the $BR_{\alpha\text{-pinene,ring-open}}$ and $BR_{\beta\text{-pinene,ring-open}}$ are substantially different from the theoretical calculations. This has been discussed in the main text.

From the above calculation, we find that $BR_{RONO2,\beta\text{-}OH,3rd}$ is about four times larger than $BR_{RONO2,ring\text{-}open}$. This result is consistent with experimentally observed products distribution in β-pinene system. From Figure 4b, it can be inferred that

$$\frac{\text{yield of endoperoxide hydroxy nitrate } (C_{10}H_{17}NO_6) \text{ at } \tau_{\text{bimolecular}} = 10 \text{ s}}{\text{yield of ring} - \text{opened hydroxy nitrate } (C_{10}H_{17}NO_4) \text{ at } \tau_{\text{bimolecular}} = 0.001 \text{ s}} = 2$$

At $\tau_{bimolecular}$ = 10 s, unimolecular reaction dominates the fate of β-pinene ring-opened RO_2, roughly 70% of which undergoes endo-cyclization, based on our theoretical calculations (Scheme 2C). This suggests that

$$\frac{\text{yield of endoperoxide hydroxy } RO_2\ (C_{10}H_{17}O_5) \text{ at } \tau_{\text{bimolecular}} = 10\text{ s}}{\text{yield of ring} - \text{opened } RO_2\ (C_{10}H_{17}O_3) \text{ at } \tau_{\text{bimolecular}} = 0.001\text{ s}} = 0.7$$

At $\tau_{bimolecular}$ = 10 s, roughly 56% of endoperoxide hydroxy RO_2 reacts with NO, based on MCM simulation. At $\tau_{bimolecular}$ = 0.001 s, nearly 100% of ring-opened RO_2 is expected to react with NO. Therefore,

$$\frac{\text{fraction of } C_{10}H_{17}O_5 + \text{NO at } \tau_{\text{bimolecular}} = 10\text{ s}}{\text{fraction of } C_{10}H_{17}O_3 + \text{NO at } \tau_{\text{bimolecular}} = 0.001\text{ s}} = 0.56$$

Combining the above three ratios, we estimate that

$$\frac{BR_{RONO2} \text{ of endoperoxide hydroxy } RO_2\ (C_{10}H_{17}O_5)}{BR_{RONO2} \text{ hydroxy } RO_2\ (C_{10}H_{17}O_3)} = \frac{2}{0.7 \times 0.56} = 5.1$$

As endoperoxide hydroxy RO_2 and ring-retained hydroxy RO_2 share similar structure (i.e., β-hydroxy RO_2 with two rings), we expect they have similar BR_{RONO2}. Thus, we infer $BR_{RONO2,\beta\text{-}OH,3rd}/BR_{RONO2,ring\text{-}open}$ to be 5.1, which is close to the ratio, 4.3, found by solving the system of equations.

5) $BR_{acetone}$ represents the branching ratio to form acetone. This branching ratio is calculated to be nearly zero as an earlier theoretical study suggested that the endo-cyclization has an energy barrier about 3.6 kcal mol^{-1} lower than that of acetone elimination[61].

6) The β-hydroxy alkoxy radicals (R2 and R3 in Scheme S 7) can undergo either H-shift or ring-opening. Peeters et al. assumed that 87.5% of the R2 and R3 would undergo ring-opening and subsequently produce pinonaldehyde. Our MC-TST calculations, however, suggest that H-shift of some R2 isomers can be competitive with its ring-opening reaction. F12 level of theory calculates that for the A3 and A9 (in Scheme S 2) derived alkoxy radical, the 1,5 H-shift from the methyl group (i.e., C9 points towards the ring and towards the alkoxy radical) to the alkoxy group proceeds at a rate of 1.9×10^8 s^{-1} (Table S 19). The H-shift channel is estimated to account for 35% of the fate of these alkoxy radicals. We note that the H-shift reaction is possible only for the isomers which have the alkoxy radical on the same side of the ring as the two methyl groups on the four-membered ring (i.e., A3, A5, A7, and A9 derived alkoxy radical). The H-shift from CH_2 group to

alkoxy radical may also be important, but not examined yet. Therefore, the branching ratios of R2 and R3 warrant future investigation.

7) The α-hydroxyalkylperoxy radical (R5 and R6 in Scheme S7) can undergo either thermal decomposition to produce pinonaldehyde or reaction with NO. Peeters et al. estimated thermal decomposition rate to be ~ 2000 s^{-1} at room temperature, making this reaction the dominant fate of α-hydroxyalkylperoxy in the atmosphere. However, Peeters et al. argued that in some laboratory studies where NO concentrations are of the order of 10-100 ppm, a significant fraction of α-hydroxyalkylperoxy would react with NO and lower the pinonaldehyde yield. The calculated pinonaldehyde yield is 35.7% under "laboratory conditions" (where 60% of α-hydroxyalkylperoxy undergoes thermal decomposition) and 59.5% under "ambient conditions" (where 100% of α-hydroxyalkylperoxy undergoes thermal decomposition). However, many laboratory studies have been performed under conditions close to "ambient conditions" and yet report much lower pinonaldehyde yields than the calculation. For example, Aschmann et al. quantified pinonaldehyde yield where initial NO concentration was 200 ppbv[62]. Using 9.15×10^{-12} s^{-1} as the RO_2+NO reaction rate coefficient (from MCM), roughly 98% of α-hydroxyalkylperoxy in the Aschmann et al. study undergoes thermal decomposition, a condition similar to "ambient condition" reported in Peeters et al. However, the measured yield is 28±5%, roughly a factor of two lower than that calculated in Peeters et al. Similarly, Wisthaler et al. measured the pinonaldehyde yield to be 34±9% when initial NO is in the range of 1-2ppm (i.e., ~90% of α-hydroxyalkylperoxy undergoes thermal decomposition)[63]. Therefore, the pinionaldehyde yield calculated in Peeters et al. is likely over-estimated.

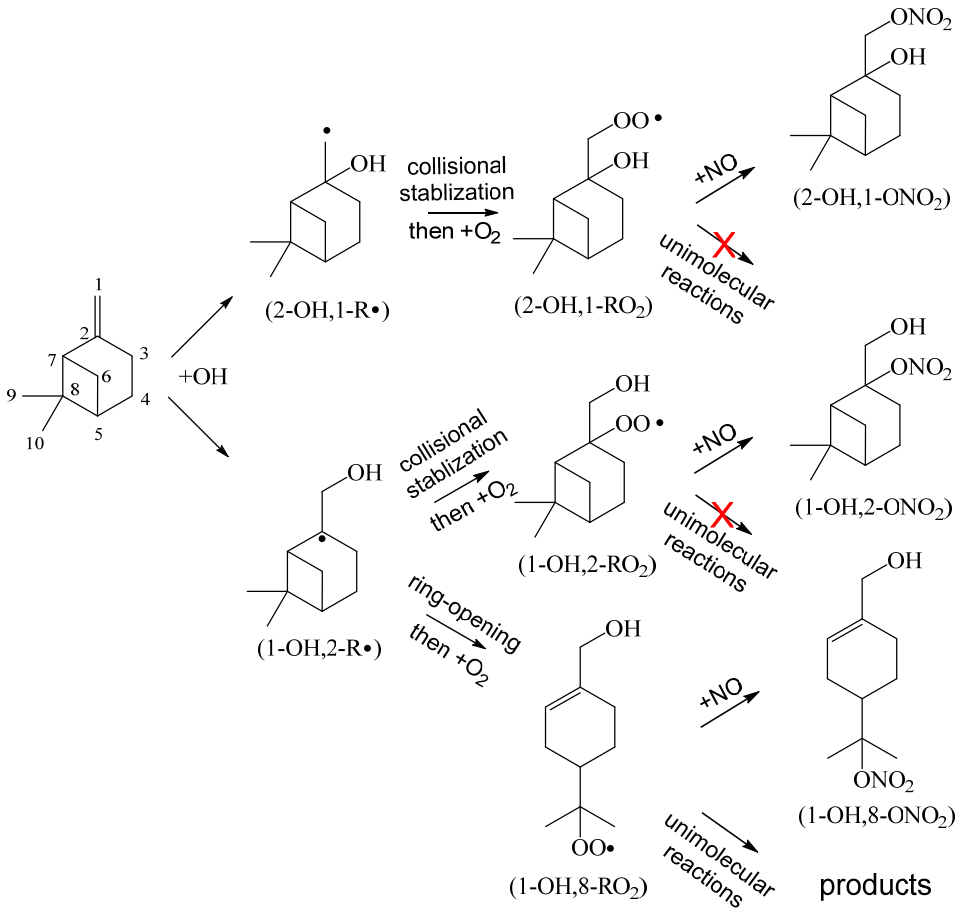

526

527 Scheme S 1. The simplified oxidation mechanism of β-pinene + OH. Each structural isomer of
528 RO_2 and hydroxy nitrate has multiple diastereoisomers, which are shown in Scheme S 2. The
529 $RO+NO_2$ produced from RO_2+NO reactions are not included in the scheme for clarity.

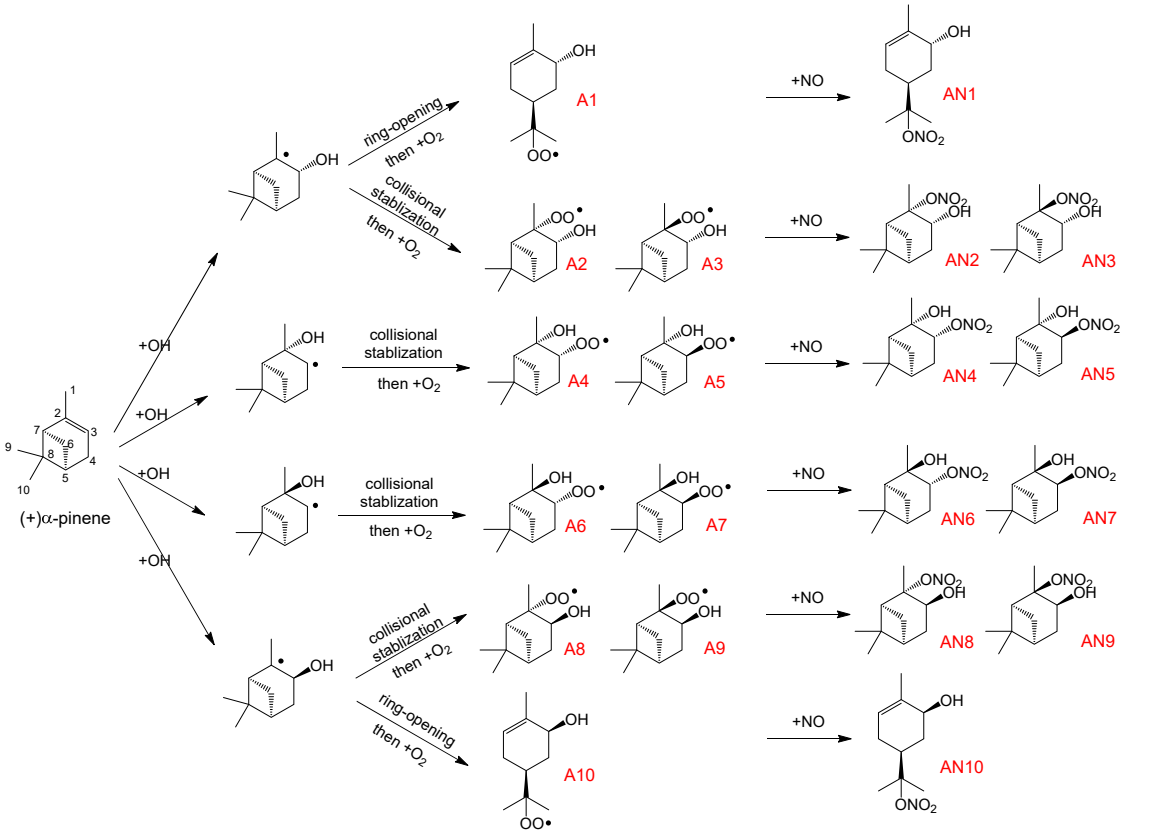

530

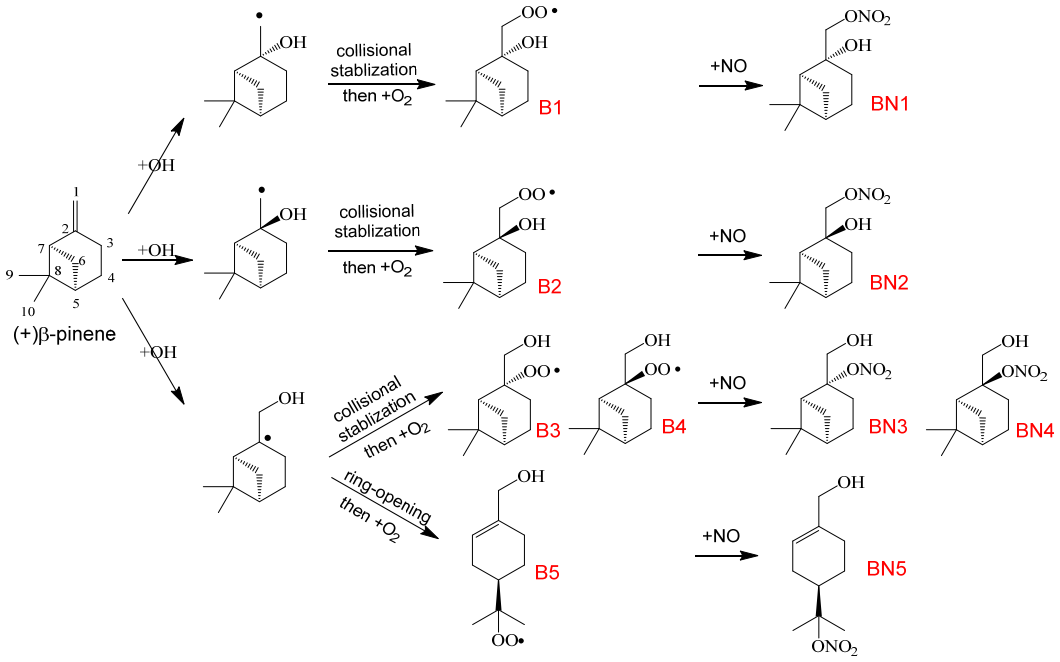

531

532 Scheme S 2. The formation of (a) ten isomers of (+) α-pinene hydroxyl nitrates (AN1-AN10) and
533 (b) five isomers of (+) β-pinene hydroxyl nitrates (BN1-BN5). (-) β-pinene is used in experiments,
534 but (+) β-pinene is used in computational calculations. The RO+NO_2 produced from RO_2+NO
535 reactions are not included in the scheme.

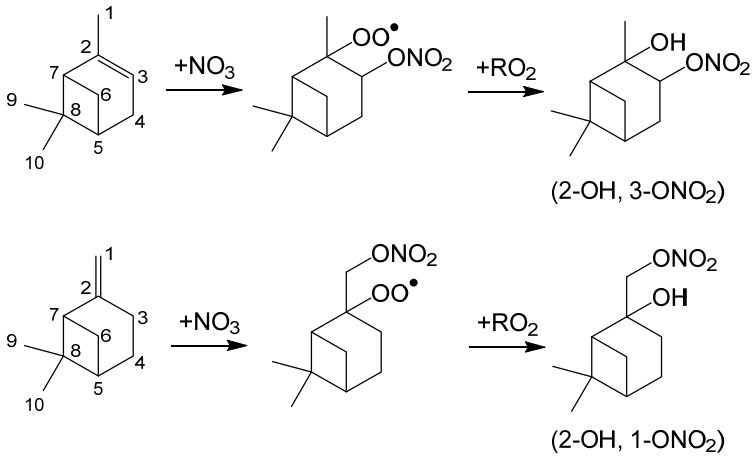

536

537 Scheme S 3. The reaction of α-pinene and β-pinene with NO_3 radical and subsequently with
538 another RO_2.

539

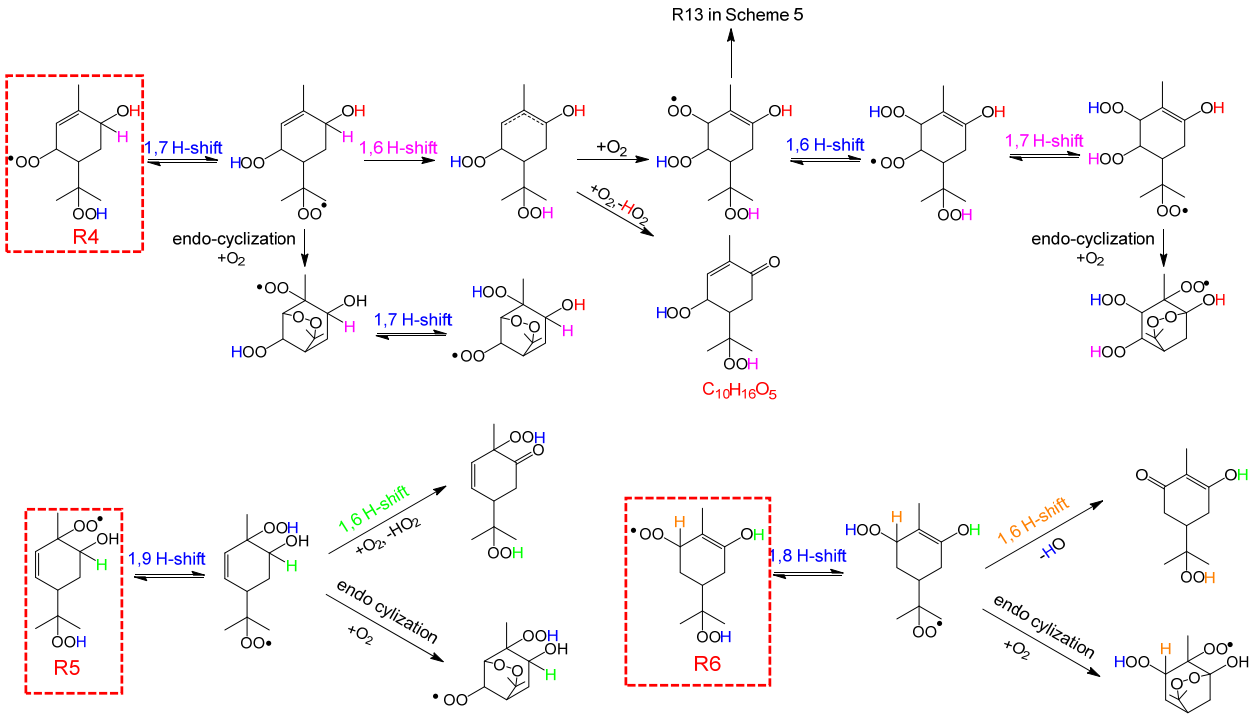

Scheme S 4. Speculations on the potential reactions of three α-pinene second-generation RO_2 (shown in red boxes). There are a number of potential reactions pathways not included in the scheme.

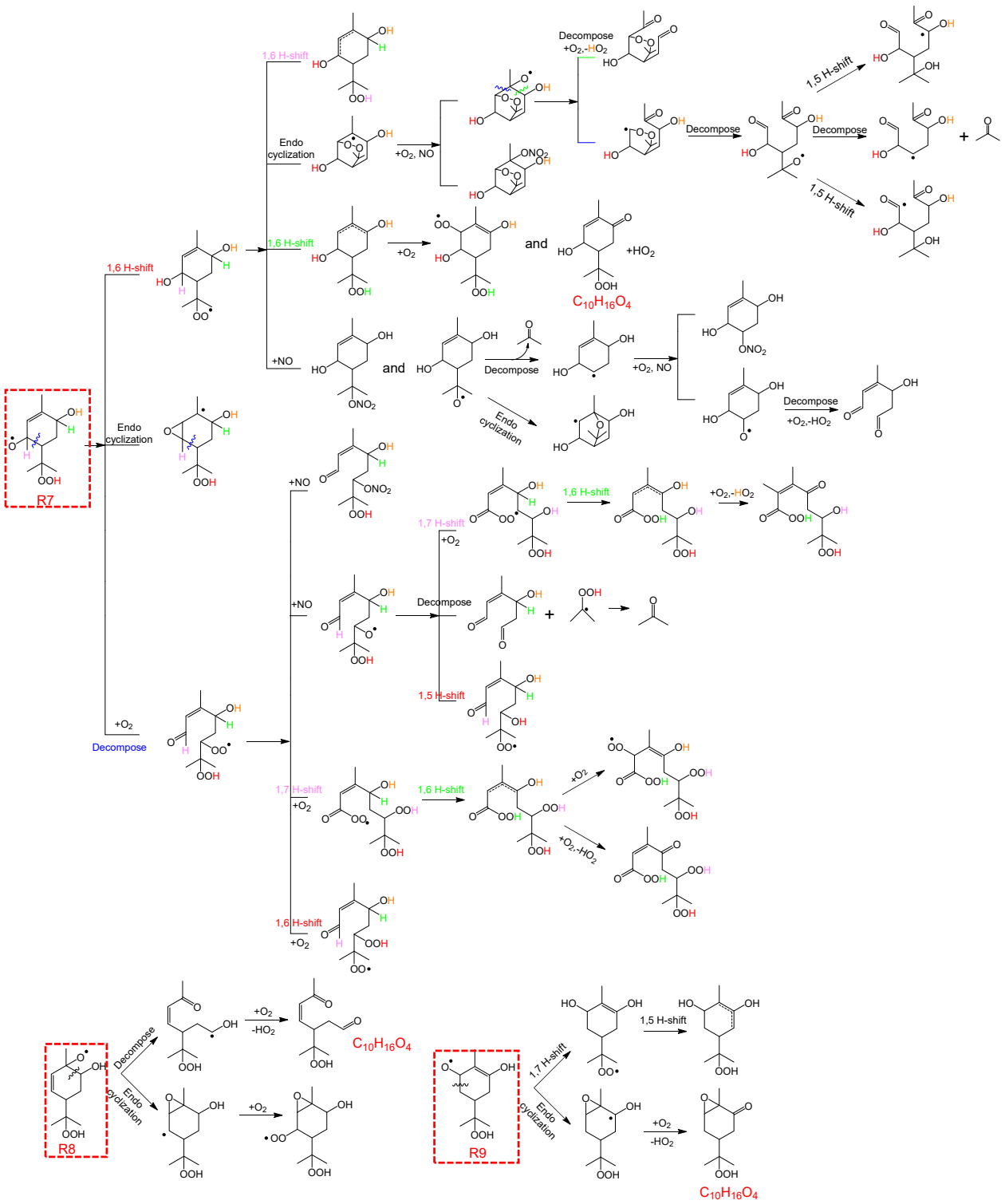

545

546 Scheme S 5. Speculations on the reactions of α-pinene second-generation alkoxy radicals (shown
547 in red boxes). There are a number of potential reactions pathways not included in the scheme.

548

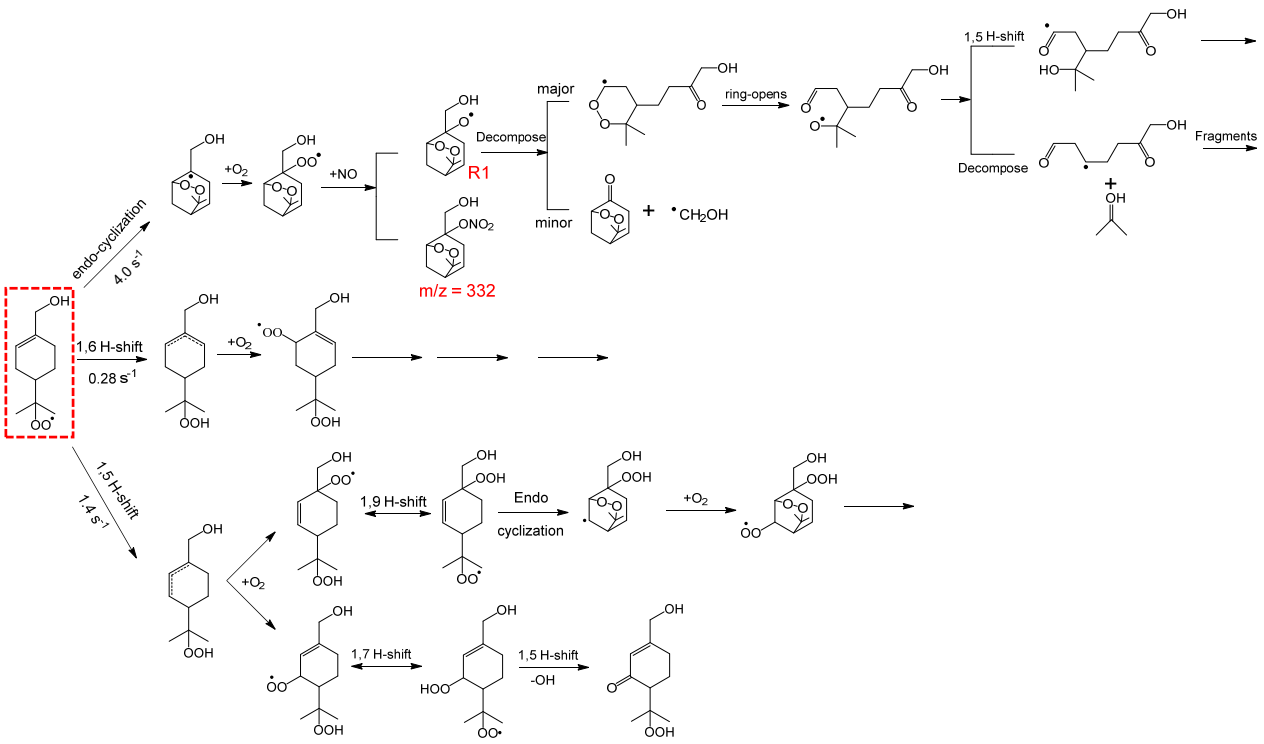

549

550 Scheme S 6. Speculations on the reactions of β-pinene 1-OH,8-RO_2 (shown in red box) following
551 the dominant initial unimolecular reactions. Rate coefficients for these are calculated using the
552 approach by Møller et al. [24]. There are a number of potential reactions pathways not included in
553 the scheme. ωB97X-D/aug-cc-pVTZ barrier heights suggest suggest that the major decomposition
554 pathway of R1 in this scheme is towards the –OO group (Table S 14).

555

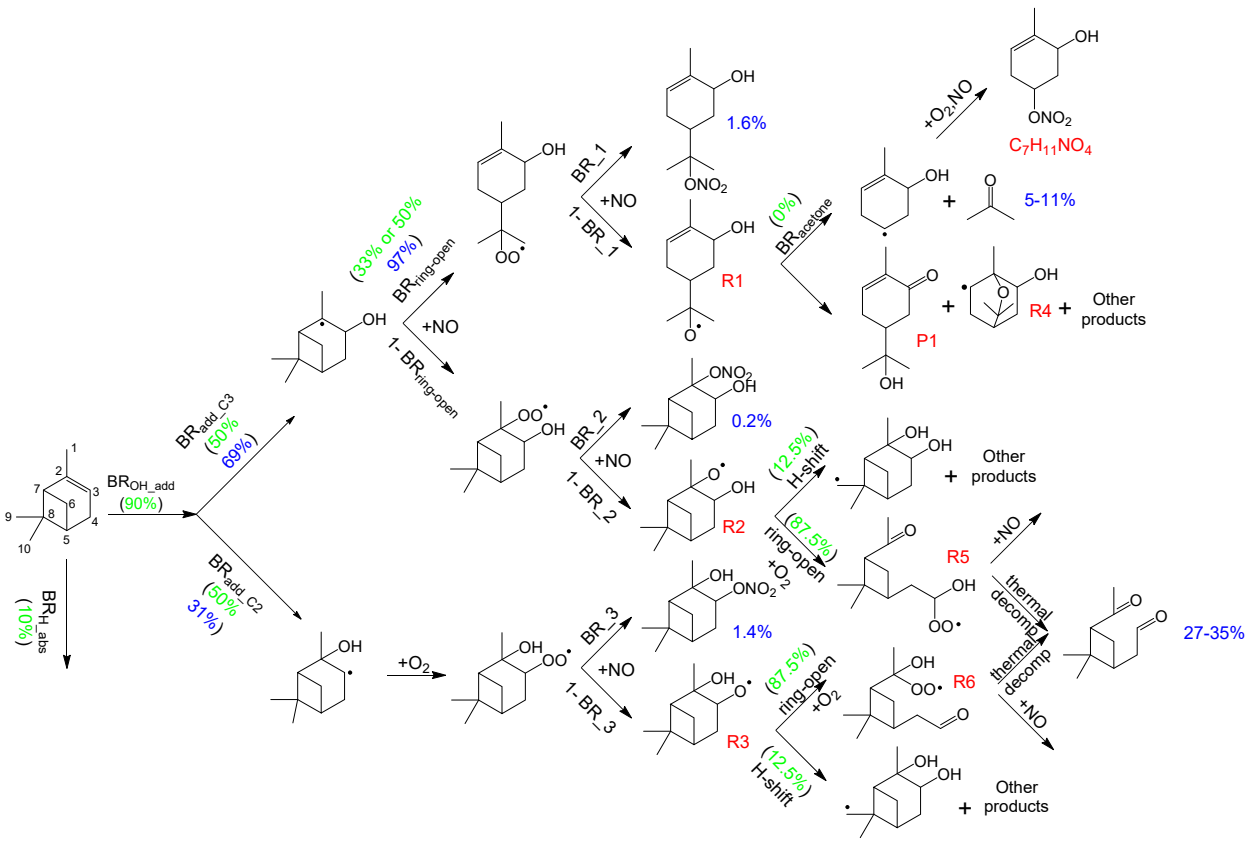

Scheme S 7. The simplified formation mechanism of hydroxy nitrates and co-products for α-pinene. The numbers marked green are from computational calculations. The numbers marked blue are experimentally constrained in this study or in the literature. The NO_2 produced from RO_2+NO is not shown in the scheme. The branching ratios of the following steps are discussed in the section S6. (1) BR_{H_abs} and BR_{OH_add} refer to the branching ratios of α-pinene reaction with OH via H abstraction and OH addition, respectively. (2) BR_{add_C2} and BR_{add_C3} refer to the branching ratios that OH addition to C2 and C3, respectively. (3) $BR_{ring\text{-}open}$ refers to the ring-opening fraction of alkyl radical. (4) "BR" refers to the nitrate branching ratio. (5) $BR_{acetone}$ refers to the branching ratio to form acetone. (6) "H-shift" and "ring-open" refer to the H-shift and ring-opening of R2 and R3. (7) "thermal decomp" and "+NO" refer to thermal decomposition and reaction with NO for R5 and R6.

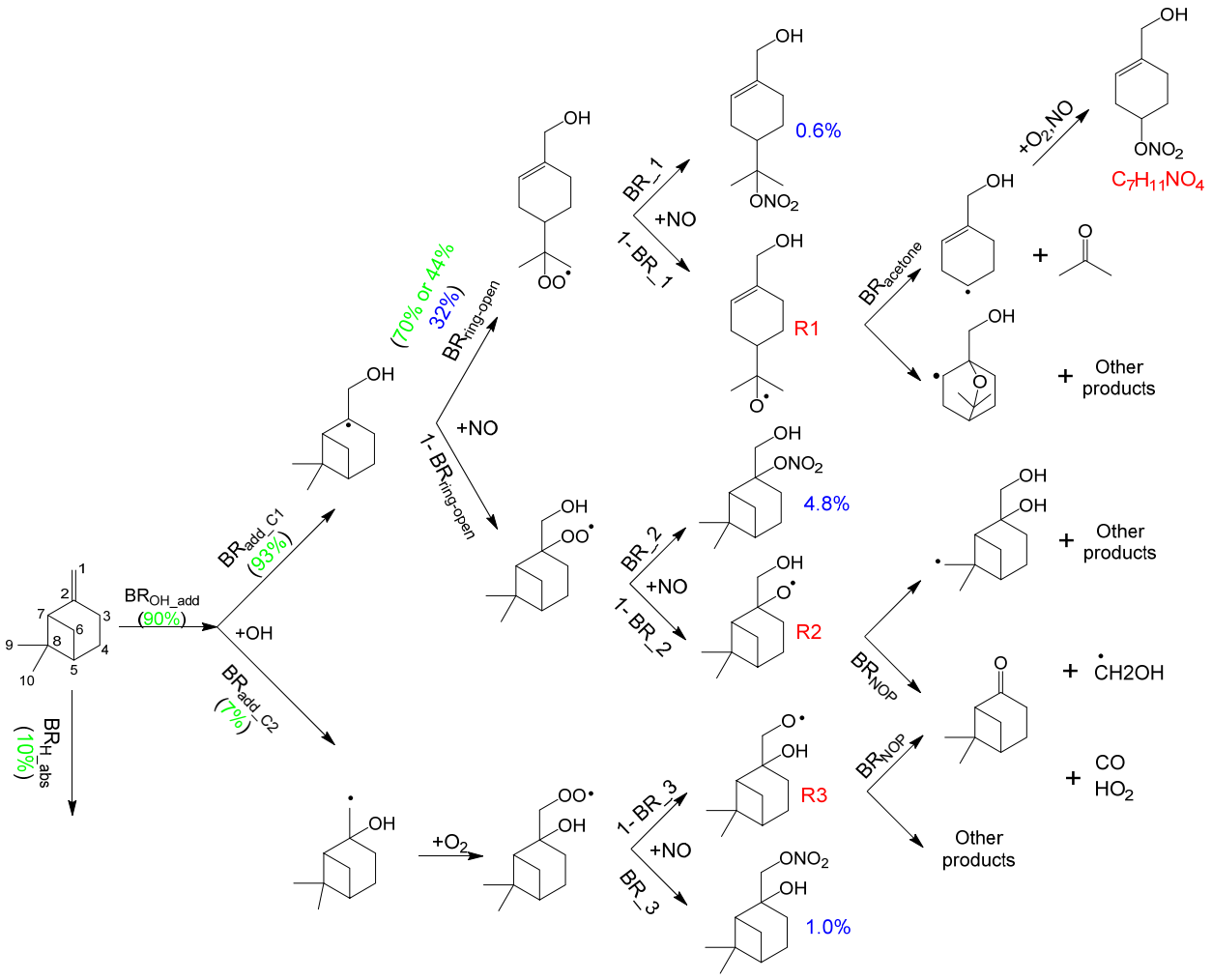

Scheme S 8. The simplified formation mechanism of hydroxy nitrates and co-products for β-pinene. The numbers marked green are from computational calculations. The numbers marked blue are experimentally constrained in this study or in the literature. The NO_2 produced from RO_2+NO is not shown in the scheme. BR_{H_abs} and BR_{OH_add} refer to the branching ratios of β-pinene reaction with OH via H abstraction and OH addition, respectively. BR_{add_C1} and BR_{add_C2} refer to the branching ratios that OH addition to C1 and C2, respectively. $BR_{ring\text{-}open}$ refers to the ring-opening fraction of alkyl radical. "BR" refers to the nitrate branching ratio (Table S 21). $BR_{acetone}$ refers to the branching ratio to form acetone. BR_{NOP} refers to the branching ratio to form nopinone.

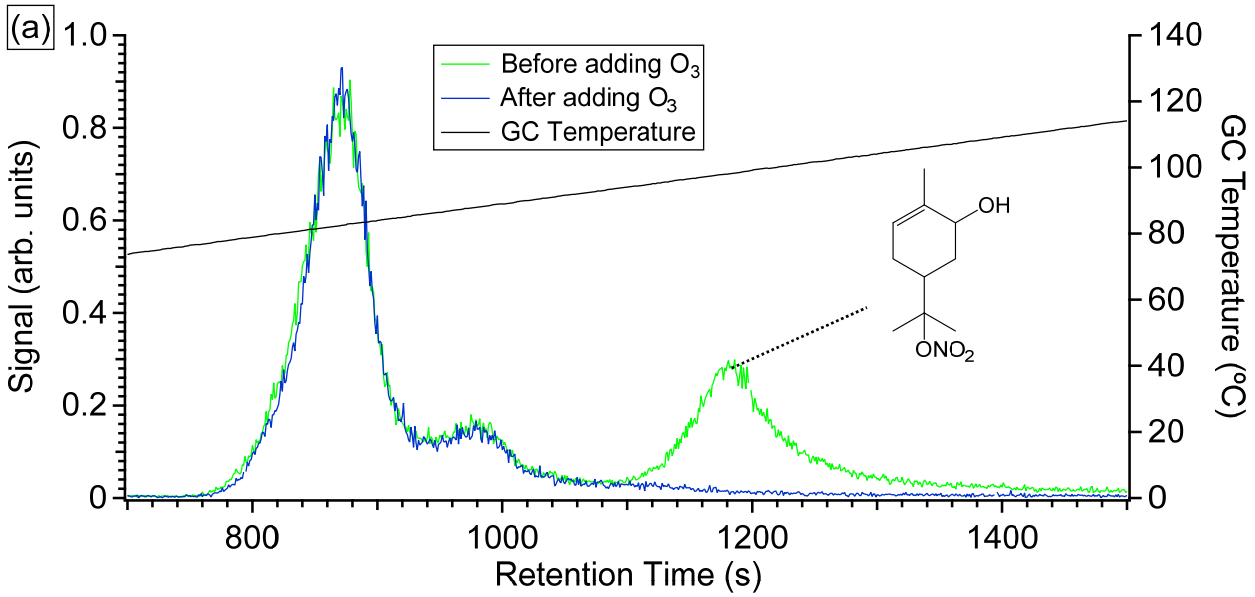

578

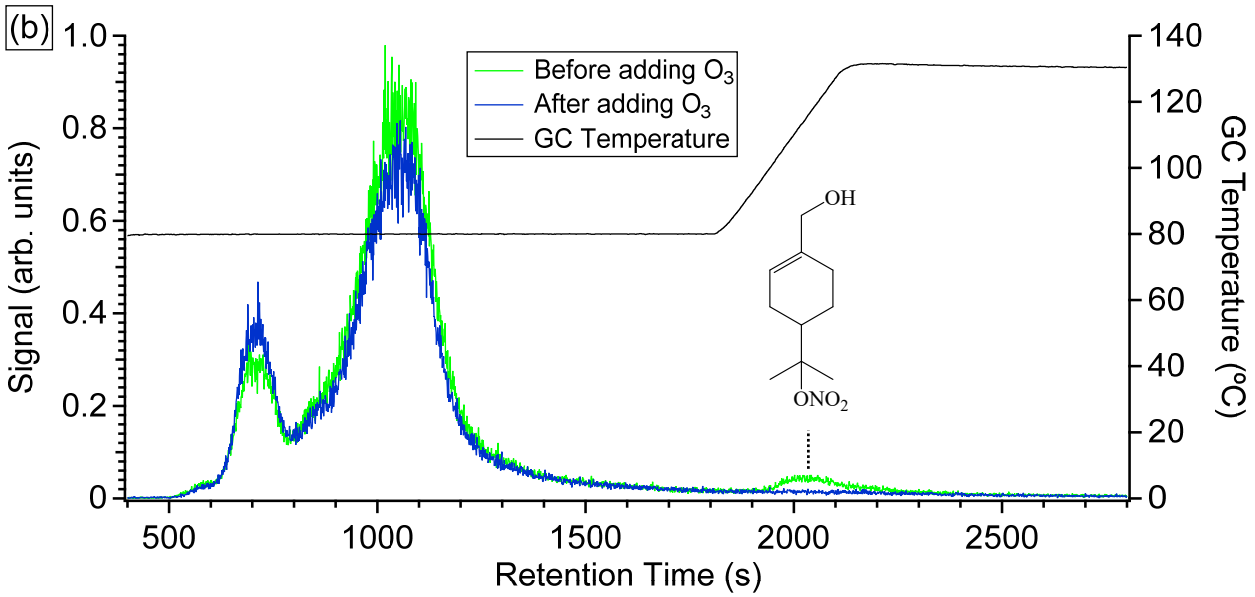

579

580 Figure S 1. The effects of adding O_3 on the distribution of (a) α-pinene and (b) β-pinene hydroxy
581 nitrates. The black lines are the GC temperature.

582

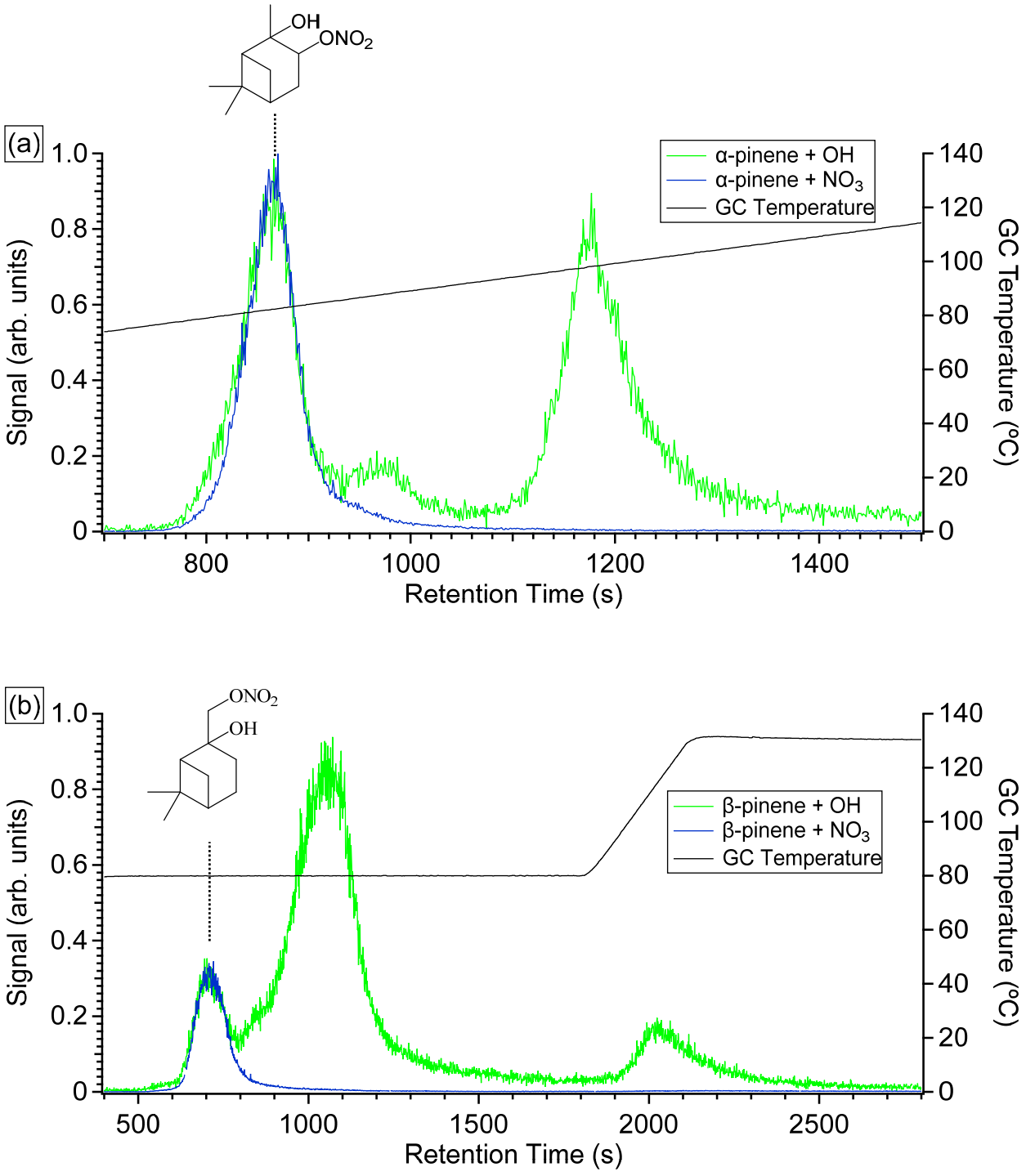

Figure S 2. The distributions of (a) α-pinene and (b) β-pinene hydroxy nitrates from OH oxidation and NO_3 oxidation. The black lines indicate the GC temperature.

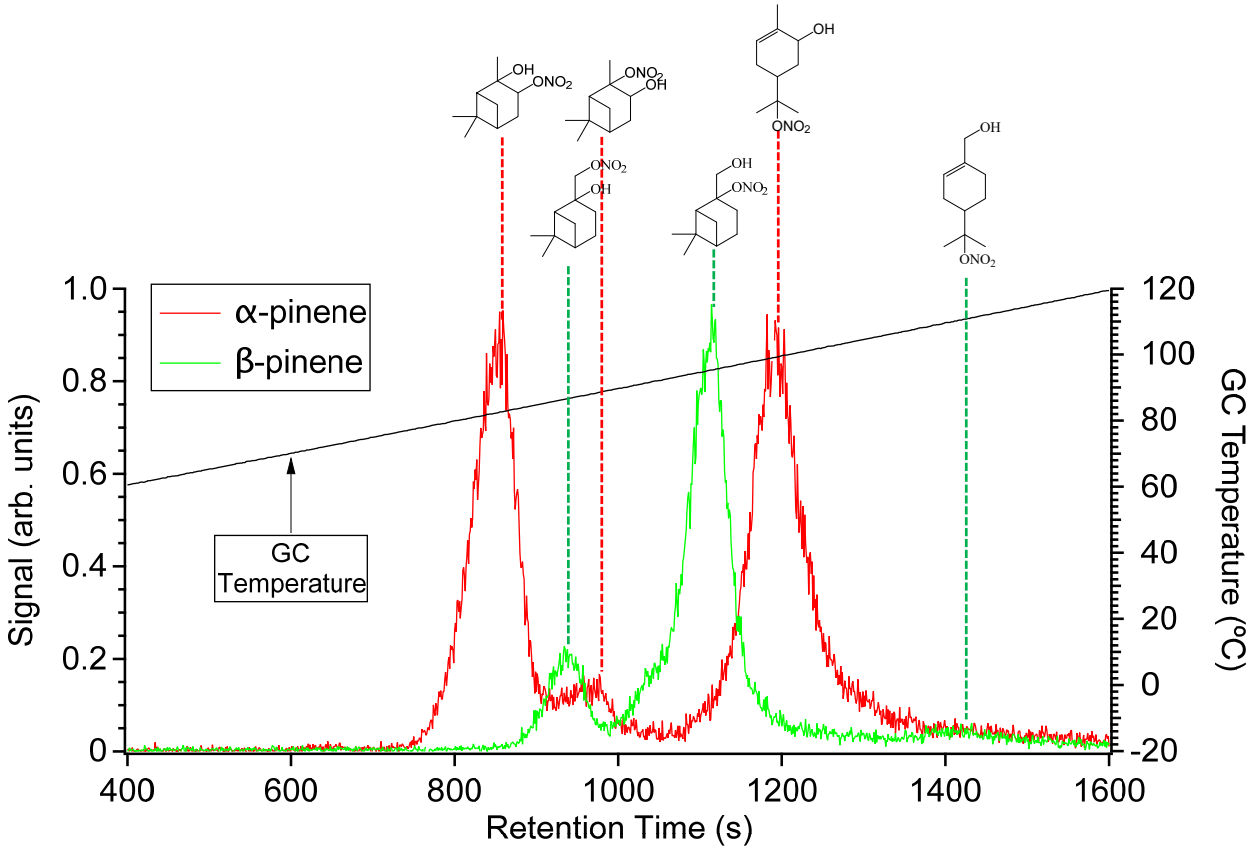

Figure S 3. The comparison between the distributions of α-pinene and β-pinene hydroxyl nitrates using the same temperature profile. The black lines indicate the GC temperature.

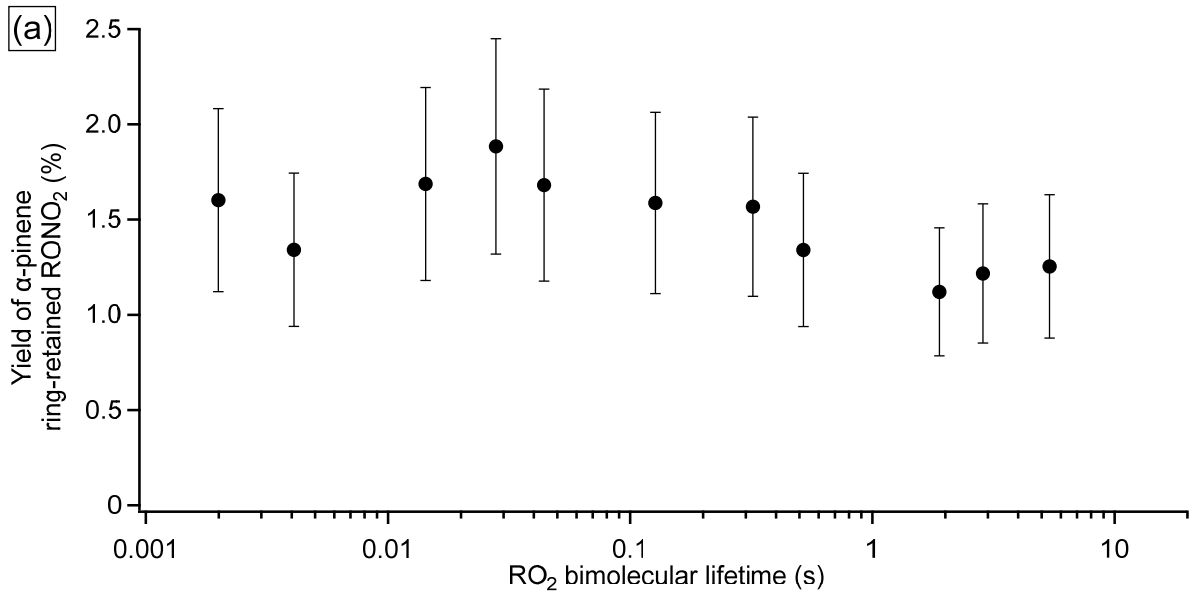

597

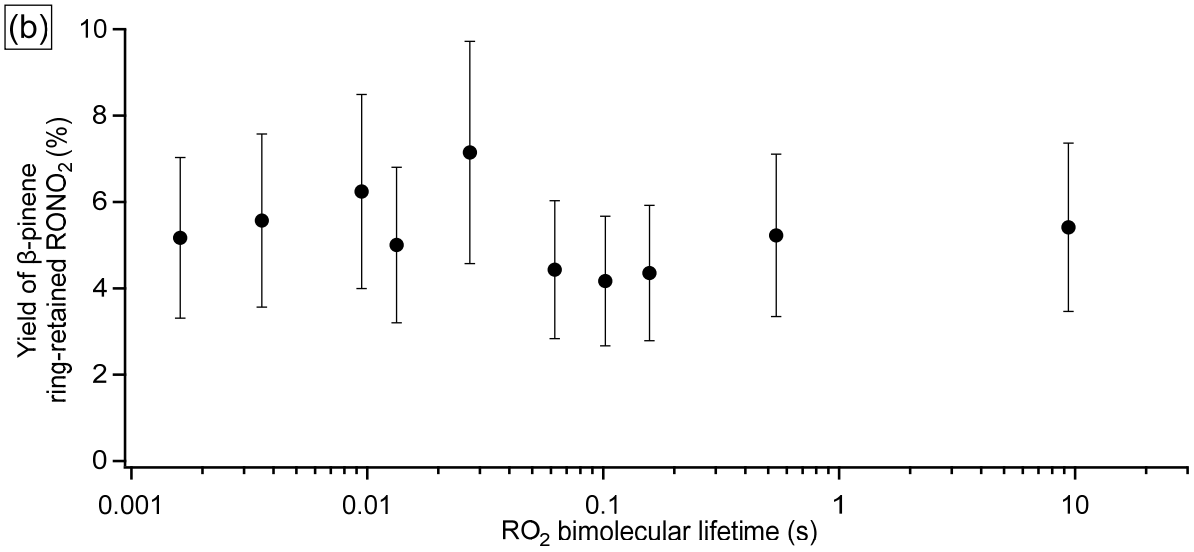

598

599 Figure S 4. The summed yield of two structural isomers of ring-retained hydroxy nitrates of (a) α-
600 pinene and (b) β-pinene as a function of RO_2 bimolecular lifetime. The ratio between two structural
601 isomers of ring-retained HNs (e.g., α-pinene 2-OH,3-ONO_2/3-OH,2-ONO_2) does not change with
602 $\tau_{bimolecular}$ (shown in Figure 1). For experiments with $\tau_{bimolecular}$ longer than 1 s, the yield is corrected
603 by the fraction of RO_2 that reacts with NO, which is estimated from MCM as described in Section
604 S2.

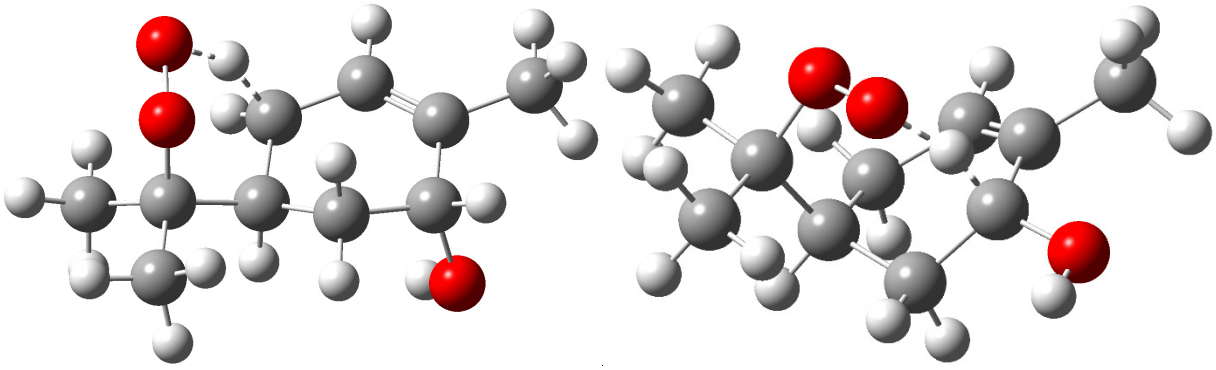

Figure S 5. Lowest-energy TS conformer for the 1,5 (left) and 1,6 (right) H-shift forming an allyl radical in the ring-opened *anti* α-pinene peroxy radical (α-pinene *anti* 3-OH,8-RO_2). The structures are optimized at the ωB97X-D/aug-cc-pVTZ level of theory. The same is observed in the *syn* α-pinene 3-OH,8RO_2 and β-pinene 1-OH,8-RO_2 systems.

(a) α-pinene *anti* 3-OH,8-RO_2 (b) α-pinene *syn* 3-OH,8-RO_2 (c) β-pinene 1-OH,8-RO_2

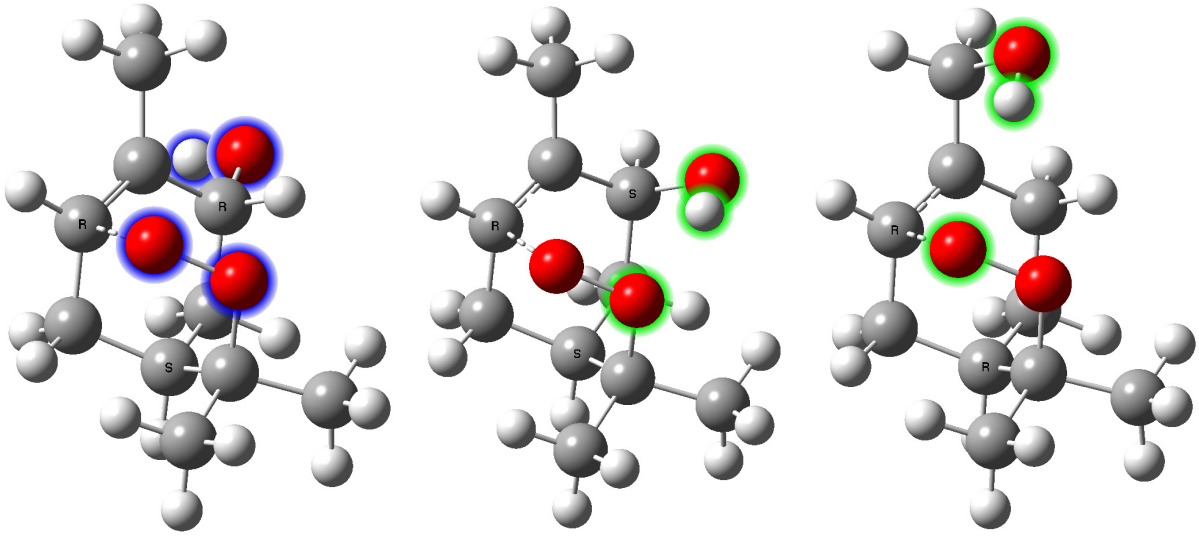

Figure S 6. The lowest-energy conformers of the TS for formation of the 6-membered endoperoxide in (a) α-pinene *anti* 3-OH,8-RO_2; (b) α-pinene *syn* 3-OH,8-RO_2 and (c) β-pinene 1-OH,8-RO_2. Green halos indicate that atoms are involved in the hydrogen bond-like interaction. Blue halos are used when no such interaction exists. We calculated (F12 electronic energy with ωB97X-D/aug-cc-pVTZ zero-point energy correction) that the barrier for ring closure is 2.5 kcal/mol larger for α-pinene *anti* 3-OH,8-RO_2 than *syn* conformer. The different H-bonding for α-pinene *anti* vs. *syn* 3-OH,8-RO_2 has previously been proposed by Vereecken et al. [61], with a calculated barrier difference (B3LYP) of ~2 kcal/mol between *anti* and *syn*.

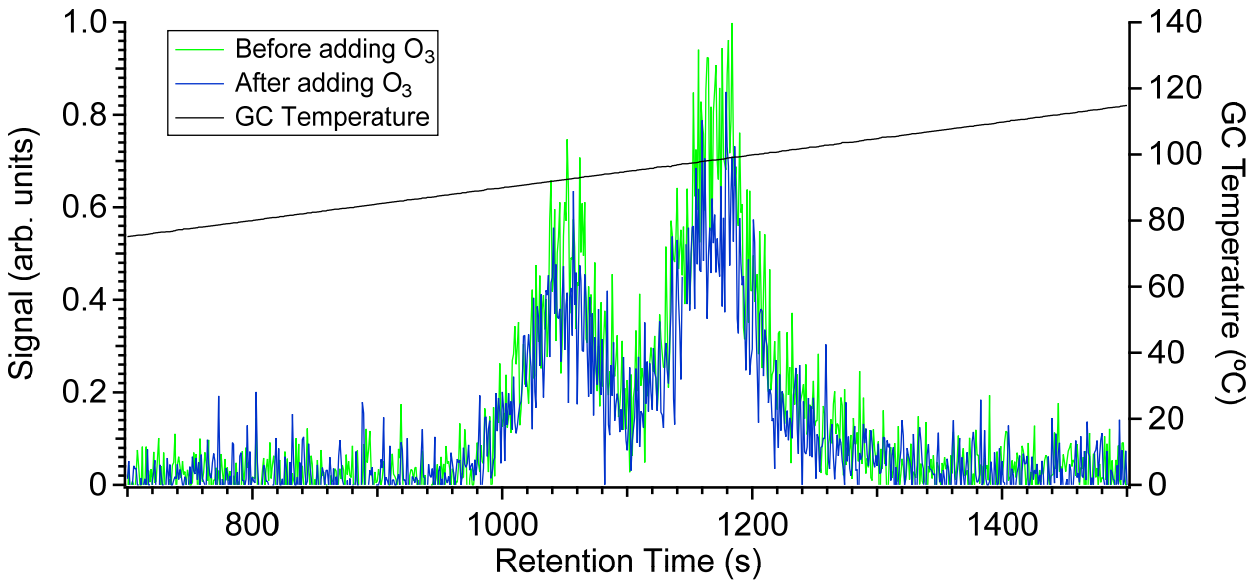

623

624 Figure S 7. The effects of adding O_3 on the *m/z* 332 from the α-pinene photooxidation. The black
625 lines are the GC temperature. Note the GC column flow is 7 sccm in this experiment, instead of 5
626 sccm in other experiments. 2.5 ppmv O_3 is added to the chamber after the photooxidation. GC is
627 taken 1 hr after adding O_3.

628

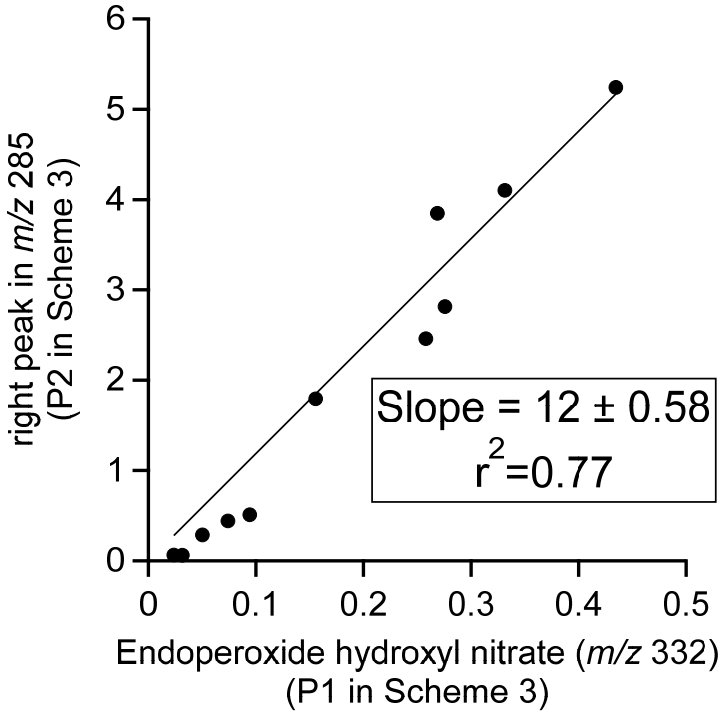

629

630 Figure S 8. The correlation between the abundances of the right peak at *m/z* 285 (in Figure 3) and
631 endoperoxide hydroxyl nitrate (*m/z* 332) in α-pinene oxidation. The signals are normalized by the
632 abundance of ring-retained HNs.

633

634

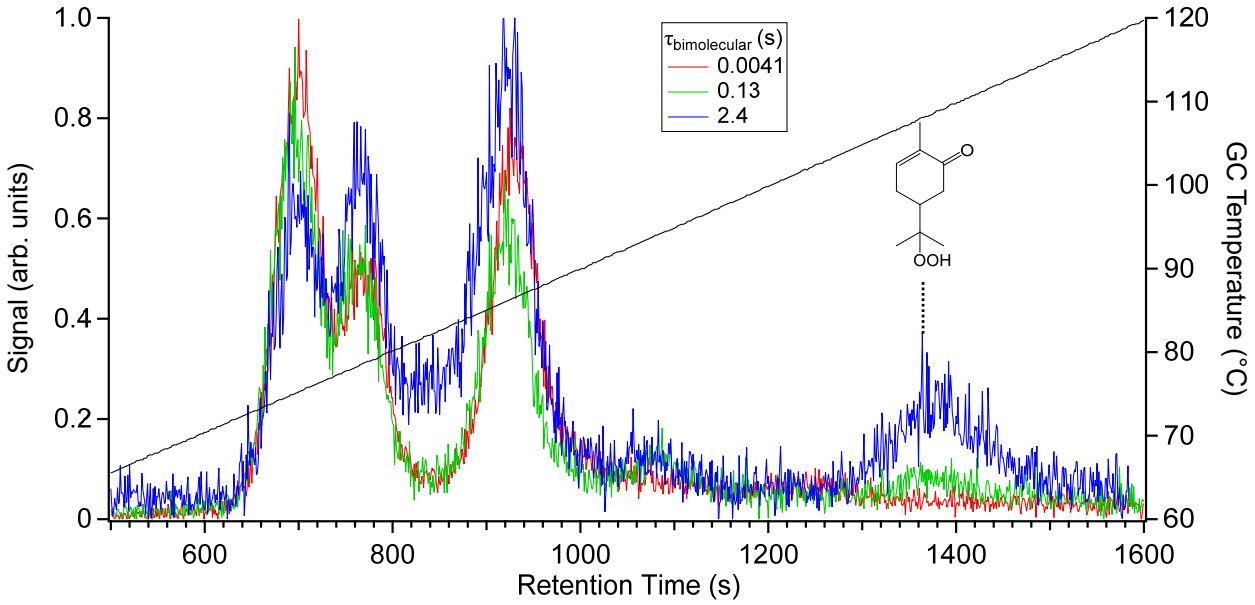

635

636 Figure S 9. GC chromatogram of *m/z* 269 in three α-pinene photooxidation experiments with
637 different RO_2 bimolecular lifetime. The signal is normalized by that of ring-retained HNs. The last
638 peak in the chromatogram is tentatively assigned to peroxide ketone (P7 in Scheme 3), mainly
639 because its signal increases with RO_2 bimolecular lifetime.

640

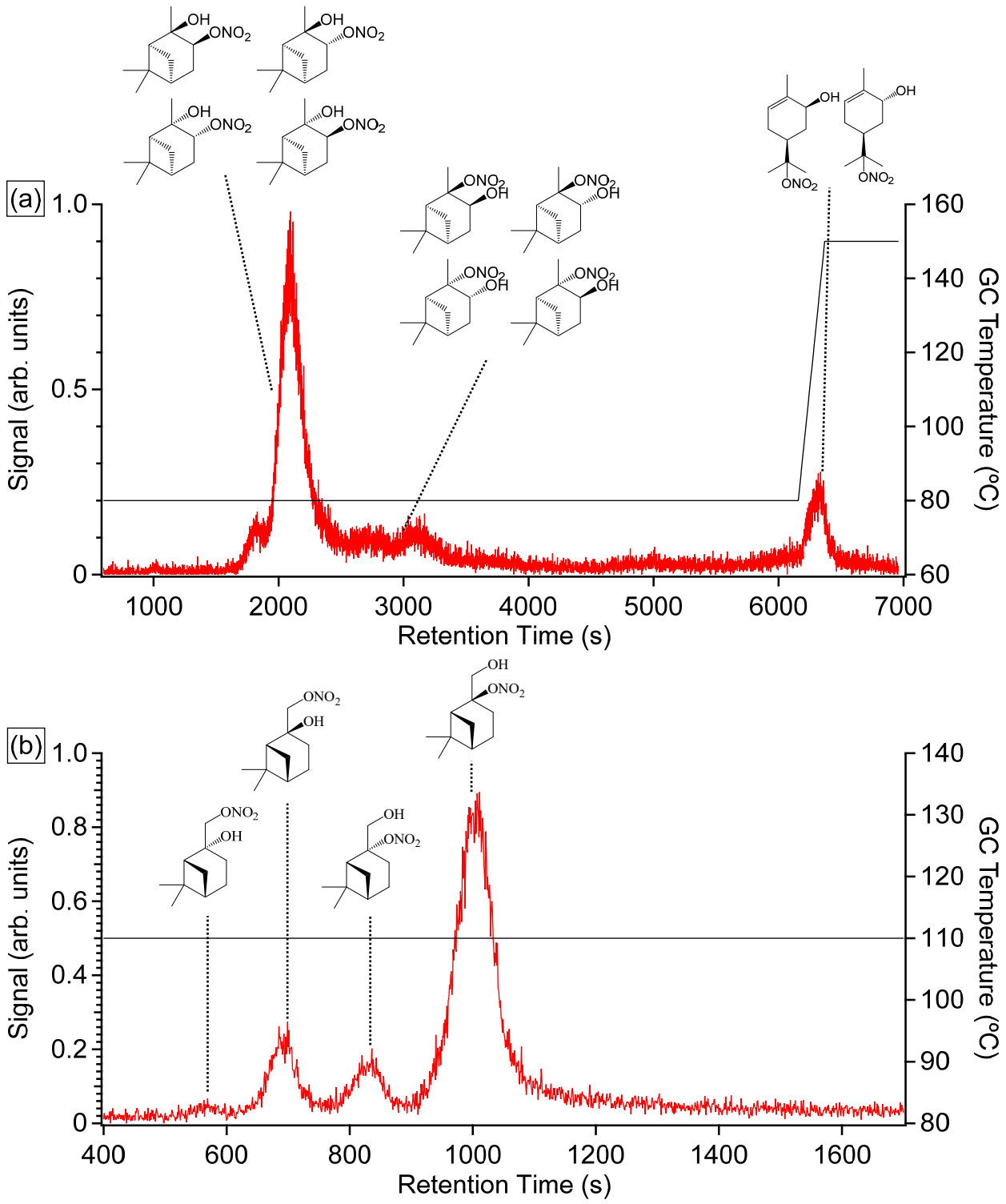

Figure S 10. The distributions of (a) α-pinene and (b) β-pinene hydroxyl nitrates using 5 m GC column. The black lines indicate the GC temperature. α-pinene hydroxy nitrate diastereomers still do not appear to be separated using the 5 m GC. Assignment of the ring-retained isomers is speculative.

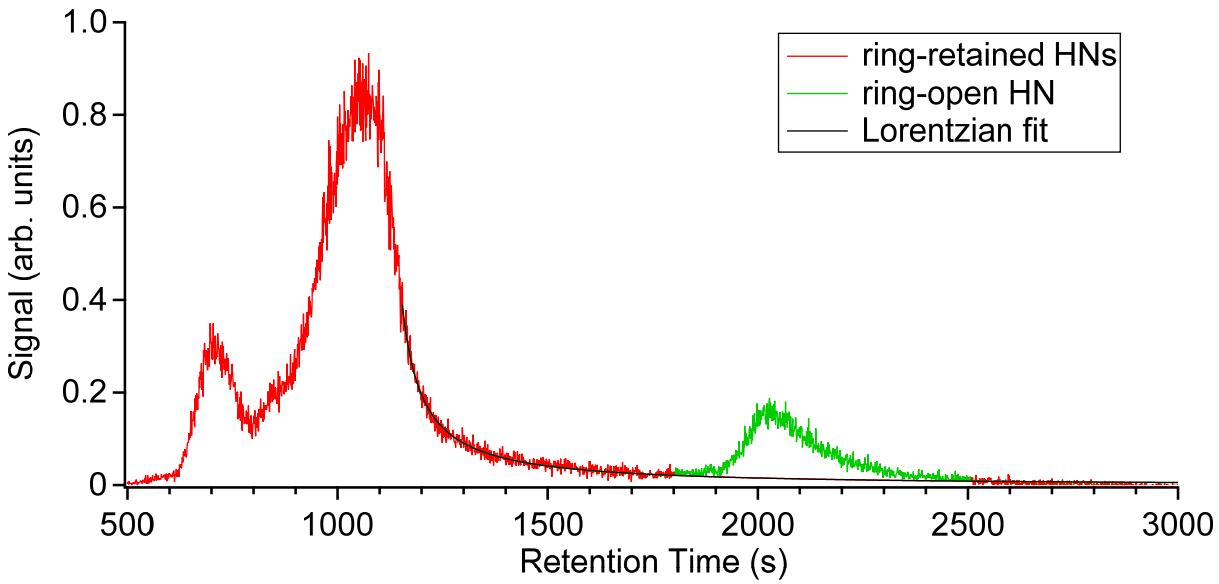

651

652 Figure S 11. The deconvolution of β-pinene hydroxy nitrates.

653

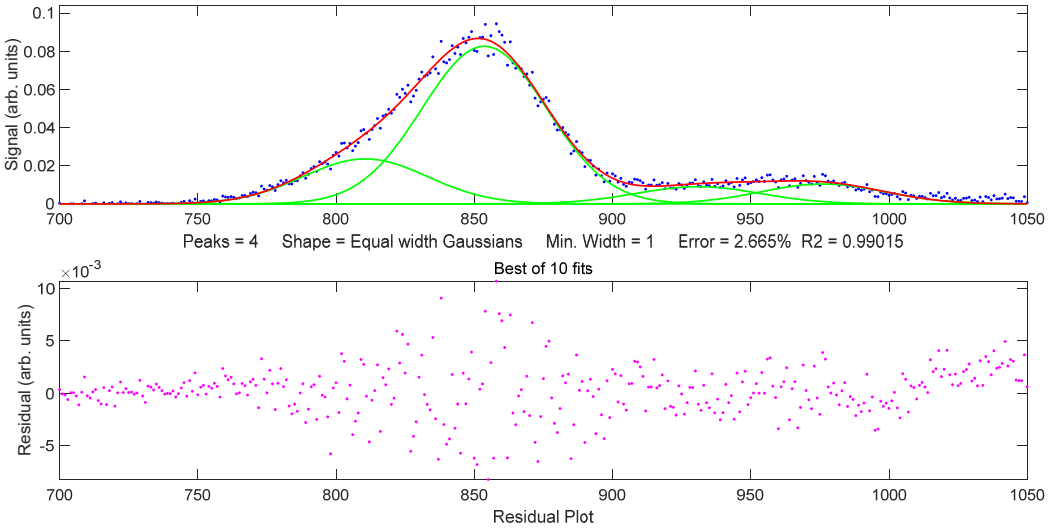

654

655 Figure S 12. The peak deconvolution using using four equal-width Gaussian functions[3] for a
656 representative α-pinene hydroxy nitrate distribution. Only the window for ring-retained HNs is
657 shown and fitted.

658

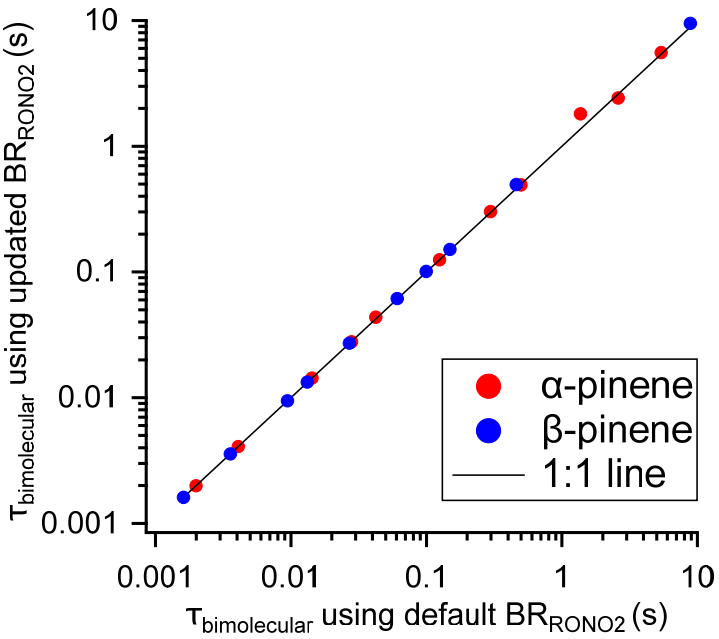

659

660 Figure S 13. $\tau_{bimolecular}$ calculated from MCM by using updated and default nitrate branching ratio.

661

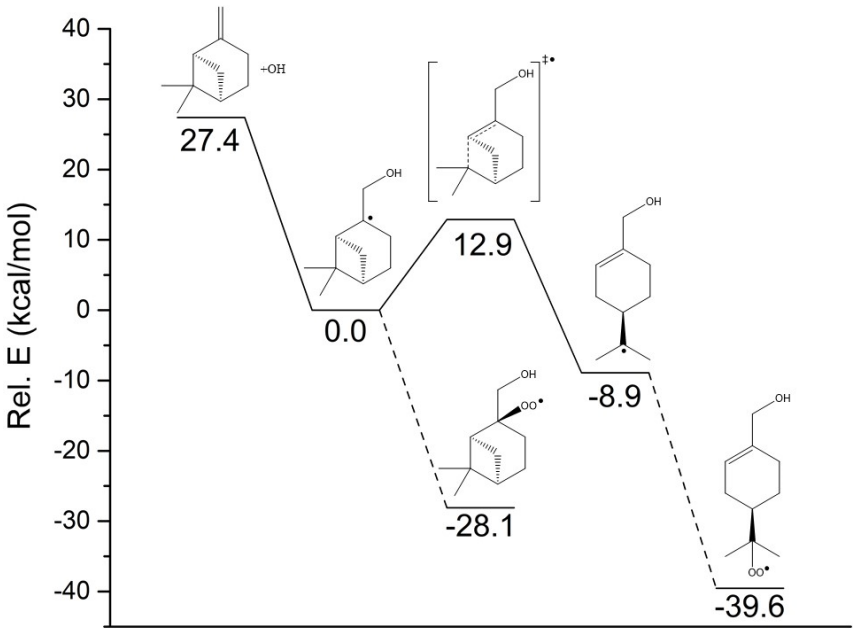

Figure S 14. System modelled for β-pinene with structures of the various compounds.

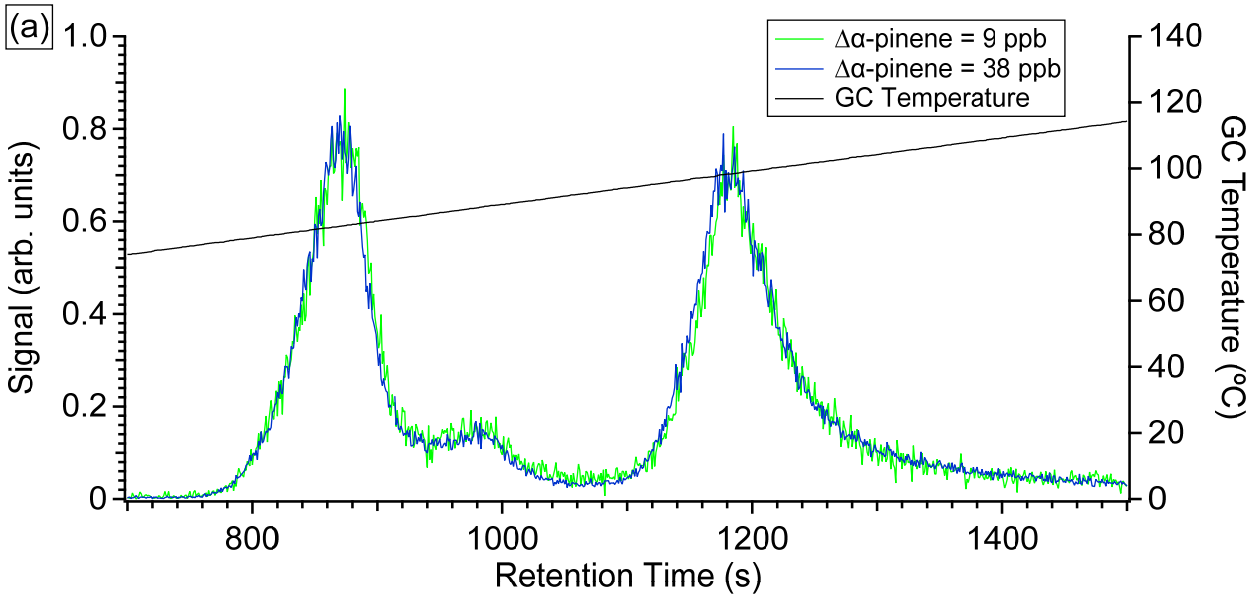

665

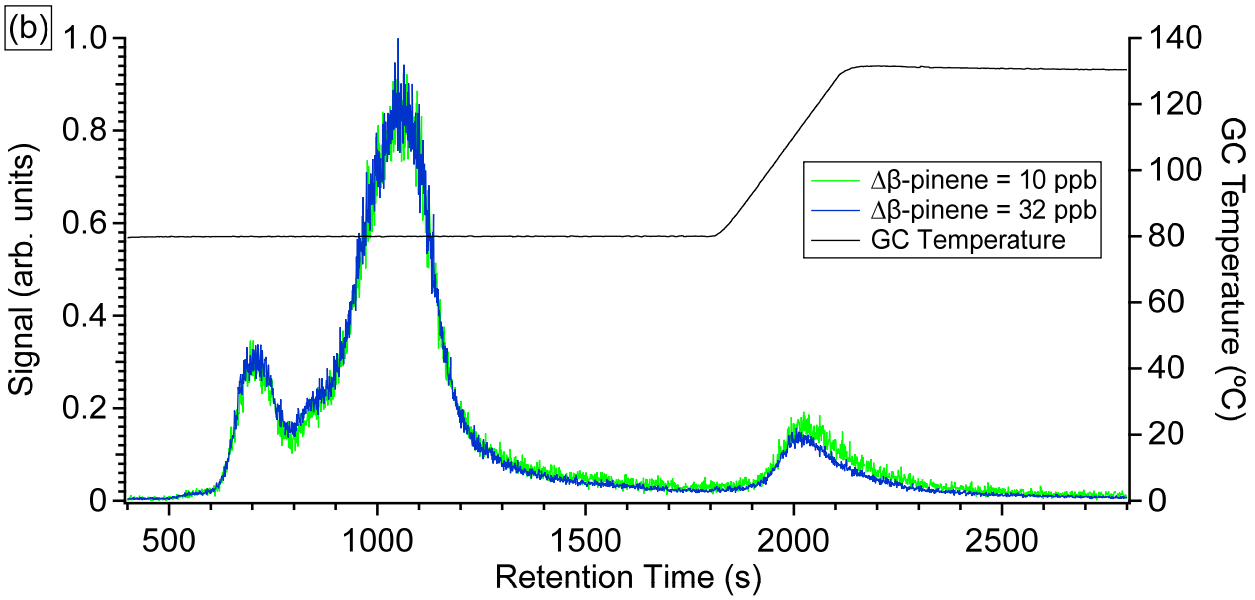

666

667 Figure S 15. The effects of gas/particle partitioning on the distribution of (a) α-pinene and (b) β-
668 pinene hydroxyl nitrates. The data are scaled to match the abundance of ring-retained hydroxy
669 nitrates. The black lines indicate the GC temperature.

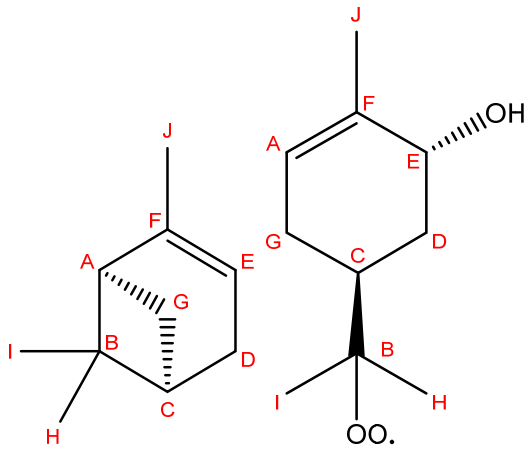

Figure S 16. Structures of α-pinene (left) and the ring-opened α-pinene peroxy radical (right) with atom labeling of the carbon atoms used to define the unimolecular reactions.

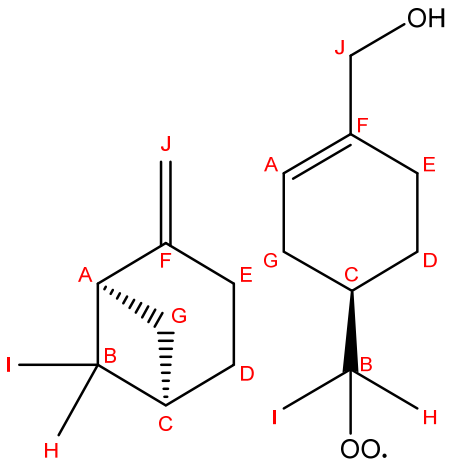

674

675 Figure S 17. Structures of β-pinene (left) and the ring-opened β-pinene peroxy radical (right) with
676 atom labeling of the carbon atoms used to define the unimolecular reactions.

677

678 Table S 1. Experimental Conditions.

VOC	Expt No.	Initial Concentration (ppbv)				Oxidation Time (min)	Reacted VOC Conc. (ppbv)	OH exposure (10^9 molec×cm^{-3}×s)
		VOC	CH_3ONO	NO	NO_2			
α-pinene	1	73.6	68.9	42.6	0.0	3.0	6.3	1.7
	2	108.0	60.2	19.8	0.0	2.5	4.7	0.8
	3	66.2	69.2	15.2	7.4	2.6	5.4	1.6
	4	66.1	62.3	5.4	2.9	5.0	3.0	0.9
	5	77.6	54.8	11.9	3.1	4.6	9.0	2.3
	6	57.7	69.9	0.0	0.0	11.0	7.8	2.7
	7	86.1	70.0	166.8	0.0	6.0	7.0	1.6
	8	82.11	68.0	320.5	0.0	10.0	8.4	2.0
	9	66.9	75.5	1100.1	0.0	30.0	7.4	2.2
	10	75.8	68.2	2241.5	94.9	15.0	7.1	1.8
	11	80.5	72.3	109.1	0.0	4.5	7.0	1.7
β-pinene	12	100.2	71.3	479.1	0.0	12.0	9.4	1.2
	13	126.3	76.5	0.0	0.0	20.0	5.2	0.5
	14	94.5	71.4	15.2	0.0	4.0	5.4	0.7
	15	109.1	75.4	80.6	0.0	5.0	8.0	1.0
	16	96.5	67.6	38.0	0.0	5.0	7.9	1.1
	17	99.7	68.9	168.9	0.0	7.0	5.5	0.7
	18	73.6	77.2	341.4	0.0	7.5	6.9	1.2
	19	73.7	76.4	52.2	0.0	4.0	7.5	1.4
	20	85.9	75.0	1253.1	0.0	20.0	9.0	1.4
	21	69.6	115.4	2773.0	0.0	20.0	6.5	1.2

679

680

Table S 2. Boltzmann averaged dipole moments (μ) and lowest-energy conformer polarizability (α) and derived collision rate (*k*) and CIMS sensitivity (*c*) of α-pinene (AN1-AN10) and β-pinene (BN1-BN5) hydroxy nitrate isomers. The structures of hydroxy nitrate isomers are shown in Scheme S 2. Dipole moments and polarizabilities are calculated at the B3LYP/cc-pVTZ level of theory.

Isomer symbol	Dipole moment μ(D)	Polarizability α ($Å^3$)	Collision rate *k* (10^{-9} cm^3 $molec^{-1}$ s^{-1})	Sensitivity *c* (10^{-4} ncts $pptv^{-1}$)
AN1	3.5	21	2.6	2.0
AN2	3.5	20	2.6	1.9
AN3	2.8	20	2.2	1.7
AN4	3.4	20	2.5	1.9
AN5	2.9	20	2.3	1.7
AN6	2.8	20	2.2	1.7
AN7	2.7	20	2.2	1.6
AN8	3.0	20	2.3	1.8
AN9	3.2	20	2.4	1.8
AN10	3.4	21	2.5	1.9
BN1	3.0	20	2.3	1.8
BN2	2.9	20	2.3	1.7
BN3	3.2	20	2.4	1.8
BN4	3.2	20	2.4	1.8
BN5	3.4	21	2.5	1.9

Table S 3. Boltzmann averaged dipole moments (μ) and lowest-energy conformer polarizability (α) and derived collision rate (*k*) and CIMS sensitivity (*c*) of α-pinene and β-pinene hydroxy hydroperoxide isomers derived from the RO_2 A1-A10 and B1-B5 (Scheme S 2). Dipole moments and polarizabilities are calculated at the B3LYP/cc-pVTZ level of theory.

Parent peroxy radical	Dipole moment μ(D)	Polarizability α ($Å^3$)	Collision rate k (10^{-9} cm^3 $molec^{-1}$ s^{-1})	Sensitivity c (10^{-4} ncts $pptv^{-1}$)
A1	2.0	19.0	1.9	1.4
A2	3.1	18.4	2.4	1.8
A3	1.4	18.5	1.6	1.2
A4	3.3	18.4	2.5	1.9
A5	1.5	18.5	1.7	1.3
A6	1.5	18.5	1.7	1.3
A7	3.3	18.4	2.5	1.9
A8	1.4	18.4	1.6	1.1
A9	3.1	18.4	2.4	1.8
A10	2.2	18.8	2.0	1.5
B1	2.8	18.4	2.2	1.7
B2	2.4	18.5	2.1	1.6
B3	2.8	18.3	2.2	1.7
B4	2.8	18.3	2.2	1.7
B5	2.1	19.1	1.9	1.5

Table S 4. Boltzmann averaged dipole moments (μ) and lowest-energy conformer polarizability (α) of glycolaldehyde (calibration reference) and endoperoxide ketoaldehyde (P2 in Scheme 3, main manuscript). All values are calculated at the B3LYP/cc-pVTZ level of theory. The sensitivity of glycolaldehyde is an experimental value serving as the reference for the remaining compounds.

Compound	Dipole moment μ(D)	Polarizability α ($Å^3$)	Collision rate k (10^{-9} cm^3 $molec^{-1}$ s^{-1})	Sensitivity c (10^{-4} ncts $pptv^{-1}$)
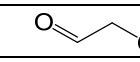	2.3	4.6	2.1	1.5
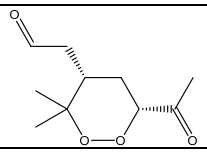	3.3	19.0	2.5	1.9

Table S 5. Boltzmann averaged dipole moments (μ) and lowest-energy conformer polarizability (α) and derived collision rate (k) and CIMS sensitivity (c) of α-pinene hydroxy hydroperoxide (OOH) and hydroxy nitrate (N) isomers derived from the RO2 A2-A4 (Scheme S 2) as well as glycolaldehyde (calibration reference). Dipole moments and polarizabilities are calculated at the B3LYP/aug-cc-pVTZ level of theory. The sensitivity of glycolaldehyde is an experimental value serving as the reference for the remaining compounds.

Compound	Dipole moment μ(D)	Polarizability α ($Å^3$)	Collision rate k (10^{-9} cm^3 $molec^{-1}$ s^{-1})	Sensitivity c (10^{-4} ncts $pptv^{-1}$)
Glycolaldehyde	2.5	5.2	2.2	1.5
A2-OOH	3.2	19.2	2.5	1.7
A3-OOH	1.4	19.3	1.7	1.1
A4-OOH	3.5	19.2	2.6	1.8
AN2	3.8	20.9	2.8	1.9
AN3	3.0	20.9	2.4	1.6
AN4	3.7	21.1	2.7	1.8

Table S 6. Calculated MC-TST reaction rate coefficients at 298.15 K for the unimolecular reactions of the hydroxy peroxy radicals formed from α-pinene + OH + O_2. Calculated using the approach by Møller et al.[24] All values are calculated at the ωB97X-D/aug-cc-pVTZ level, except for electronic energies of the lowest-energy conformers and IRC end-points, which are at the F12 level. Tunneling is based on IRC end-points. The abstraction/addition site refer to the structures in Figure S 16, with "-OH" referring to abstraction of the hydrogen from the hydroxy group on the specified carbon atom. The peroxy radicals are defined in Scheme S 2.

Peroxy radical	H-shift type	Abstraction/addition site	k (s^{-1})
A1	1,5 H-shift	G	1.1
	1,5 H-shift	D	$1.2 \cdot 10^{-6}$
	1,6 H-shift	E	0.37
	6-membered endoperoxide formation	A	0.35
	7-membered endoperoxide formation	F	$2.0 \cdot 10^{-3}$
A2	1,5-OH H-shift	E-OH	-
A4	1,5-OH H-shift	F-OH	-
A7	1,5-OH H-shift	F-OH	-
A9	1,5-OH H-shift	E-OH	-
A10	1,5 H-shift	G	0.16
	1,5 H-shift	D	$8.8 \cdot 10^{-6}$
	1,7-OH H-shift	E-OH	-
	6-membered endoperoxide formation	A	2.3
	7-membered endoperoxide formation	F	$2.6 \cdot 10^{-2}$

Table S 7. Calculated MC-TST reaction rate coefficients at 298.15 K for the unimolecular reactions of the hydroxy peroxy radicals formed from β-pinene + OH + O_2. Calculated using the approach by Møller et al.[24] All values are calculated at the ωB97X-D/aug-cc-pVTZ level, except for electronic energies of the lowest-energy conformers and IRC end-points, which are at the F12 level. Tunneling is based on IRC end-points. The abstraction/addition site refer to the structures in Figure S 17, with "-OH" referring to abstraction of the hydrogen from the hydroxy group on the specified carbon atom. The peroxy radicals are defined in Scheme S 2.

Peroxy radical	Reaction type	Abstraction/addition site	k (s^{-1})
B1	1,5-OH H-shift	F-OH	-
B2	1,5 H-shift	E	$8.1 \cdot 10^{-2}$
	1,5-OH H-shift	F-OH	-
B3	1,5-OH H-shift	J-OH	-
B4	1,5-OH H-shift	J-OH	-
B5	1,5 H-shift	G	1.4
	1,5 H-shift	D	$7.3 \cdot 10^{-6}$
	1,6 H-shift	E	$2.8 \cdot 10^{-1}$
	6-membered Endoperoxide formation	A	4.0
	7-membered Endoperoxide formation	F	$4.8 \cdot 10^{-2}$

Table S 8. Calculated MC-TST reaction rate coefficients at 298.15 K for the unimolecular reactions of the hydroxy peroxy radicals formed from α-pinene + OH + O_2. All values are calculated at the ωB97X-D/aug-cc-pVTZ level of theory with tunneling based on IRC end-points. The abstraction/addition site refer to the structures in Figure S 16, with "-OH" referring to abstraction of the hydrogen from the hydroxy group on the specified carbon atom. The peroxy radicals are defined in Scheme S 2.

Peroxy radical	H-shift type	Abstraction/addition site	k (s^{-1})
A1	1,5 H-shift	G	0.66[a]
	1,5 H-shift	D	$3.0 \cdot 10^{-7}$
	1,6 H-shift	E	0.96[a]
	6-membered endoperoxide formation	A	$7.9 \cdot 10^{-2}$ [a]
	7-membered endoperoxide formation	F	$1.1 \cdot 10^{-4}$
A2	1,5-OH H-shift	E-OH	$4.7 \cdot 10^{-2}$
A4	1,5-OH H-shift	F-OH	$2.8 \cdot 10^{-2}$
A7	1,5-OH H-shift	F-OH	$1.2 \cdot 10^{-2}$
A9	1,5-OH H-shift	E-OH	0.12
A10	1,5 H-shift	G	0.41
	1,5 H-shift	D	$8.3 \cdot 10^{-7}$
	1,7-OH H-shift	E-OH	$1.9 \cdot 10^{-9}$
	6-membered endoperoxide formation	A	0.95
	7-membered endoperoxide formation	F	$1.9 \cdot 10^{-3}$

[a] Also reported in Berndt et al.[43]

Table S 9. Calculated reaction rate coefficients at 298.15 K for the unimolecular reactions of the hydroxy peroxy radicals formed from β-pinene + OH + O_2. All values are calculated at the ωB97X-D/aug-cc-pVTZ level of theory with tunneling based on IRC end-points. The abstraction/addition site refer to the structures in Figure S 17, with "-OH" referring to abstraction of the hydrogen from the hydroxy group on the specified carbon atom. The peroxy radicals are defined in Scheme S 2.

Peroxy radical	Reaction type	Abstraction/addition site	k (s^{-1})
B1	1,5-OH H-shift	F-OH	$5.3 \cdot 10^{-4}$
B2	1,5 H-shift	E	$1.9 \cdot 10^{-2}$
	1,5-OH H-shift	F-OH	$1.6 \cdot 10^{-2}$
B3	1,5-OH H-shift	J-OH	$2.6 \cdot 10^{-4}$
B4	1,5-OH H-shift	J-OH	$1.8 \cdot 10^{-3}$
B5	1,5 H-shift	G	0.63
	1,5 H-shift	D	$2.7 \cdot 10^{-6}$
	1,6 H-shift	E	0.13
	6-membered Endoperoxide formation	A	0.34
	7-membered Endoperoxide formation	F	$1.5 \cdot 10^{-3}$

Table S 10. Calculated reaction rate coefficients at 298.15 K for the unimolecular reactions of the hydroxy peroxy radicals formed from α-pinene + OH + O_2. All values are calculated at the B3LYP/6-31+G(d) level of theory with tunneling assuming thermoneutral reactions. The abstraction/addition site refer to the structures in Figure S 16, with "-OH" referring to abstraction of the hydrogen from the hydroxy group on the specified carbon atom. The peroxy radicals are defined in Scheme S 2. The reactions highlighted in bold are the ones also treated at a higher level of theory.

Peroxy radical	Reaction type	Abstraction/addition site	k (s^{-1})
A1	**1,5 H-shift**	**G**	**63**
	1,5 H-shift	**D**	**$1.8 \cdot 10^{-4}$**
	1,6 H-shift	**E**	**52**
	1,6 H-shift	A	$3.5 \cdot 10^{-17}$
	1,7-OH H-shift	E-OH	$9.4 \cdot 10^{-16}$
	6-membered endoperoxide formation	**A**	**2.7**
	7-membered endoperoxide formation	**F**	**$1.7 \cdot 10^{-3}$**
A2	1,4 H-shift	A	$2.9 \cdot 10^{-10}$
	1,5 H-shift	D	$8.5 \cdot 10^{-15}$
	1,4 H-shift	E	$5.8 \cdot 10^{-20}$
	1,5-OH H-shift	**E-OH**	**2.1**
	1,5 H-shift	G	$3.6 \cdot 10^{-3}$
	1,4 H-shift	J	$8.2 \cdot 10^{-9}$
A3	1,4 H-shift	A	$6.0 \cdot 10^{-11}$
	1,5 H-shift	D	$8.0 \cdot 10^{-19}$
	1,4 H-shift	E	$5.1 \cdot 10^{-4}$
	1,5-OH H-shift	E-OH	$2.2 \cdot 10^{-7}$
	1,6 H-shift	I	$1.1 \cdot 10^{-7}$
	1,4 H-shift	J	$1.3 \cdot 10^{-9}$
A4	1,4 H-shift	D	$2.8 \cdot 10^{-7}$
	1,5-OH H-shift	**F-OH**	**7.4**
	1,6 H-shift	G	$1.2 \cdot 10^{-7}$
A5	1,4 H-shift	D	$4.3 \cdot 10^{-8}$
	1,5 H-shift	J	$5.0 \cdot 10^{-5}$
	1,5-OH H-shift	F-OH	$1.9 \cdot 10^{-5}$
	1,7 H-shift	I	$5.0 \cdot 10^{-8}$
A6	1,4 H-shift	D	$3.1 \cdot 10^{-7}$
	1,5 H-shift	J	$4.7 \cdot 10^{-5}$
	1,5-OH H-shift	F-OH	$5.3 \cdot 10^{-6}$
	1,6 H-shift	G	$7.1 \cdot 10^{-8}$
A7	1,4 H-shift	D	$1.4 \cdot 10^{-8}$

	1,5 H-shift	J	$2.9 \cdot 10^{-8}$
	1,5-OH H-shift	**F-OH**	**3.5**
	1,7 H-shift	I	$2.7 \cdot 10^{-6}$
A8	1,4 H-shift	A	$1.3 \cdot 10^{-10}$
	1,5 H-shift	D	$1.2 \cdot 10^{-19}$
	1,4 H-shift	E	$1.9 \cdot 10^{-3}$
	1,5-OH H-shift	E-OH	$6.5 \cdot 10^{-7}$
	1,5 H-shift	G	$1.3 \cdot 10^{-10}$
	1,4 H-shift	J	$2.5 \cdot 10^{-9}$
A9	1,4 H-shift	A	$1.2 \cdot 10^{-11}$
	1,5 H-shift	D	$6.4 \cdot 10^{-16}$
	1,4 H-shift	E	$2.8 \cdot 10^{-23}$
	1,5-OH H-shift	**E-OH**	**75**
	1,6 H-shift	I	$1.6 \cdot 10^{-4}$
	1,4 H-shift	J	$8.9 \cdot 10^{-10}$
A10	**1,5 H-shift**	**G**	**2.5**
	1,5 H-shift	**D**	$\mathbf{6.9 \cdot 10^{-6}}$
	1,7-OH H-shift	**E-OH**	$\mathbf{5.2 \cdot 10^{-5}}$
	6-membered endoperoxide formation	**A**	**20**
	7-membered endoperoxide formation	**F**	$\mathbf{3.1 \cdot 10^{-2}}$

749

750

Table S 11. Calculated reaction rate coefficients at 298.15 K for the unimolecular reactions of the hydroxy peroxy radicals formed from β-pinene + OH + O_2. All values are calculated at the B3LYP/6-31+G(d) level of theory with tunneling assuming thermoneutral reactions. The abstraction/addition site refer to the structures in Figure S 17, with "-OH" referring to abstraction of the hydrogen from the hydroxy group on the specified carbon atom. The peroxy radicals are defined in Scheme S 2. The reactions highlighted in bold are the ones also treated at a higher level of theory.

Peroxy radical	Reaction type	Abstraction/addition site	k (s^{-1})
B1	1,5 H-shift	A	$5.1 \cdot 10^{-4}$
	1,6 H-shift	D	$6.1 \cdot 10^{-15}$
	1,5 H-shift	E	$1.6 \cdot 10^{-3}$
	1,5-OH H-shift	**F-OH**	**0.61**
	1,7 H-shift	I	$1.1 \cdot 10^{-4}$
B2	1,5 H-shift	A	$4.8 \cdot 10^{-4}$
	1,6 H-shift	D	$2.7 \cdot 10^{-11}$
	1,5 H-shift	**E**	$\mathbf{1.9 \cdot 10^{-2}}$
	1,5-OH H-shift	**F-OH**	**22**
	1,6 H-shift	G	$5.2 \cdot 10^{-6}$
B3	1,4 H-shift	A	$6.3 \cdot 10^{-11}$
	1,5 H-shift	D	$4.4 \cdot 10^{-19}$
	1,4 H-shift	E	$1.9 \cdot 10^{-6}$
	1,5 H-shift	G	$2.4 \cdot 10^{-5}$
	1,4 H-shift	J	$6.3 \cdot 10^{-4}$
	1,5-OH H-shift	**J-OH**	**0.81**
B4	1,4 H-shift	A	$2.4 \cdot 10^{-5}$
	1,5 H-shift	D	$3.2 \cdot 10^{-17}$
	1,4 H-shift	E	$5.1 \cdot 10^{-7}$
	1,6 H-shift	I	$4.3 \cdot 10^{-6}$
	1,4 H-shift	J	$7.0 \cdot 10^{-4}$
	1,5-OH H-shift	**J-OH**	**0.87**
B5	**1,5 H-shift**	**G**	**2.7**
	1,5 H-shift	**D**	$\mathbf{8.7 \cdot 10^{-7}}$
	1,6 H-shift	**E**	**0.12**
	1,9-OH H-shift	J-OH	$3.3 \cdot 10^{-10}$
	6-membered endoperoxide formation	**A**	**8.3**
	7-membered endoperoxide formation	**F**	$\mathbf{2.7 \cdot 10^{-2}}$

Table S 12. Imaginary frequency (ν_{imag}, cm^{-1}) of the lowest-energy TS, reaction and IRC barriers (kcal/mol), approximate Eckart tunneling coefficient calculated assuming a thermoneutral reaction ($\kappa_{thermoneutral}$) and Eckart tunneling coefficients calculated using the optimized IRC end-points (κ_{IRC}). Values are given for the unimolecular reactions of the B5 peroxy radical. All values are calculated using B3LYP/6-31+G(d). The abstraction/addition site refer to the structures in Figure S 17.

Reaction	Abstraction/ addition site	ν_{imag}	Reaction barrier[1]	Forward IRC barrier	Reverse IRC barrier	$\kappa_{thermoneutral}{}^{2}$	$\kappa_{IRC}{}^{3}$
1,5 H-shift	G	1819i	17.84	16.33	13.39	173.44	99.80
1,5 H-shift	D	1676i	25.72	24.42	4.58	164.19	10.72
1,6 H-shift	E	1738i	18.92	13.61	10.40	118.97	41.82
1,9-OH H-shift	J-OH	1322i	27.98	22.67	3.52	13.13	4.39
6-membered endoperoxide formation	A	492i	13.49	8.93	8.36	1.29	1.29
7-membered endoperoxide formation	F	448i	16.53	11.97	7.79	1.23	1.23

[1] Energy difference (Ee+ZPVE) between lowest-energy reactant and TS conformer

[2] Eckart tunneling coefficient calculated using the imaginary frequency and assuming both the forward and reverse IRC barriers are equal to the reaction barrier of the forward reaction.

[3] Eckart tunneling coefficient calculated using the imaginary frequency and the forward and reverse barriers obtained from optimized end-points of the forward and reverse IRC from the lowest-energy TS.

Table S 13. ωB97X-D/aug-cc-pVTZ calculated barrier heights (electronic energy and zero-point correction, kcal/mol) between lowest-energy conformers for the possible bond scission pathways of α-pinene R2 (Scheme 3, main manuscript).

Isomer	Breaking towards -OO (left)	Breaking towards OH (right)
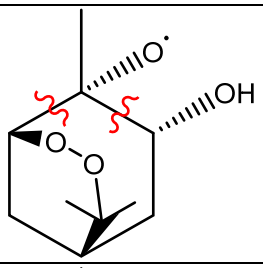	6.2	3.0
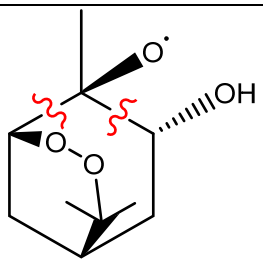	7.3	3.9
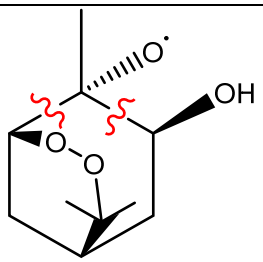	6.5	2.8
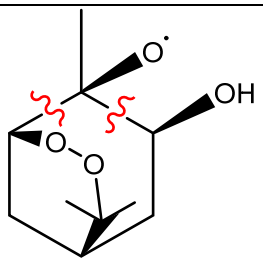	3.4	3.4

779 Table S 14. ωB97X-D/aug-cc-pVTZ calculated barrier heights (electronic energy and zero-point
780 correction, kcal/mol) between lowest-energy conformers for the possible bond scission pathways
781 of β-pinene R1 (Scheme S 6).

Isomer	Bond scission towards -OO (left)	Bond scission towards CH_2 (right)	Bond scission towards CH_2OH (up)
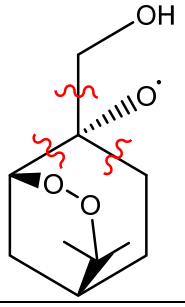	2.8	8.9	6.2
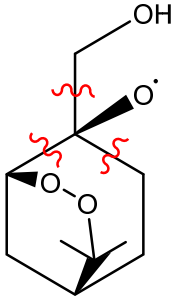	4.5	9.8	7.2

782

783

Table S 15. Structures formed by OH-addition to α-pinene and β-pinene of the three hydroxy alkyl radicals which may potentially ring-open. For each, the amount of excess energy relative to the free reactants, the barrier for ring-opening, the calculated canonical MC-TST rate coefficient and the fraction ring-opening and adding O_2 is given. Electronic energies for the important species are calculated using F12 and all other values using ωB97X-D/aug-cc-pVTZ.

Name	Structure	Excess energy (kcal/mol)	Barrier (kcal/mol)	Canonical rate coefficients (s^{-1})	Fraction ring-opening	Fraction adding O_2
α-pinene-OH I	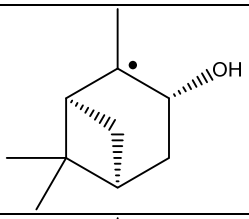	27.96	13.29	9.9×10^{2}	0.33	0.67
α-pinene-OH II	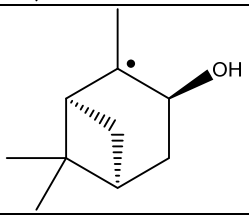	27.53	13.20	5.5×10^{2}	0.31	0.69
β-pinene-OH	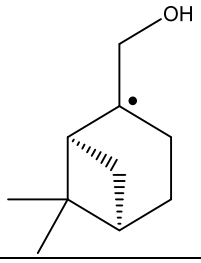	27.45	12.89	2.2×10^{3}	0.44	0.56

Table S 16. Reaction parameters of the three hydroxy alkyl radicals formed by OH-addition to α-pinene and β-pinene which may potentially ring-open. For each, the amount of excess energy relative to the free reactants, the barrier for ring-opening, the calculated canonical MC-TST rate coefficient and the fraction ring-opening and adding O_2 is given. All values are calculated using ωB97X-D/aug-cc-pVTZ.

Name	Excess energy (kcal/mol)	Barrier (kcal/mol)	Canonical rate coefficients (s^{-1})	Fraction ring-opening	Fraction adding O_2
α-pinene-OH I	31.16	14.47	6.4×10^{1}	0.24	0.76
α-pinene-OH II	30.59	14.21	1.0×10^{2}	0.25	0.75
β-pinene-OH	30.54	13.90	1.7×10^{2}	0.37	0.63

798 Table S 17. Fraction ring-opening before O_2-addition with the ring-opening barrier height changed
799 by ±1 kcal/mol. Everything else is as in Table S 15.

Name	Barrier -1 kcal/mol	Barrier +1 kcal/mol
α-pinene-OH I	0.59	0.15
α-pinene-OH II	0.57	0.15
β-pinene-OH	0.71	0.23

800

801

802 Table S 18. Fraction ring-opening before O_2-addition with the energy transfer per collision (ΔE_{down})
803 either decreased or increased by 75 cm^{-1}. Everything else is as in Table S 15.

Name	ΔE_{down} = 150 cm^{-1}	ΔE_{down} = 300 cm^{-1}
α-pinene-OH I	0.49	0.24
α-pinene-OH II	0.47	0.23
β-pinene-OH	0.62	0.34

804

805

Table S 19. MC-TST reaction rate coefficients (s^{-1}) for three competing reactions of two ring-retained α-pinene hydroxy alkoxy radicals. The barrier height is calculated using either ωB97X-D/aug-cc-pVTZ or F12 and all other values are calculated using ωB97X-D/aug-cc-pVTZ. Includes an Eckart tunneling correction for all reactions. This H-shift reaction is possible only for the isomers which have the alkoxy radical on the same side of the ring as the methyl groups on the four-membered ring and the H-shift can only occur from the methyl group pointing towards the alkoxy radical.

	Theory for barrier height	1,5 H-shift	Bond scission towards 4-membered ring (left)	Bond scission towards OH-group (right)
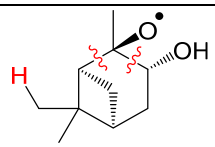	ωB97X-D	2.1×10^{8}	9.1×10^{5}	6.2×10^{10}
	F12	1.9×10^{8}	-	3.5×10^{8}
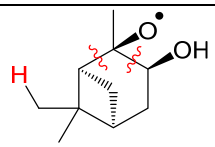	ωB97X-D	4.2×10^{8}	6.5×10^{4}	2.1×10^{9}
	F12	1.9×10^{8}	-	3.5×10^{8}

Table S 20. The signals of even mass between 200 and 360 relative to *m/z* 300 in an α-pinene experiment with $\tau_{bimolecular}$ ~0.004 s^{-1}. Only *m/z* with signal accounting for more than 1% of that of *m/z* 300 is included in the table. The isotope abundance of major odd mass (253, 269, and 285) has been subtracted from relevant *m/z*'s (254, 270, and 286).

m/z	Signal relative to *m/z* 300	*m/z*	Signal relative to *m/z* 300
300	1.00	282	0.02
316	0.25	264	0.02
330	0.13	216	0.02
302	0.13	304	0.02
286	0.11	246	0.02
318	0.10	270	0.02
298	0.09	212	0.02
314	0.09	278	0.02
258	0.08	210	0.02
274	0.05	332	0.02
262	0.05	242	0.02
254	0.04	260	0.01
256	0.04	202	0.01
222	0.04	320	0.01
248	0.03	346	0.01
288	0.03	266	0.01
230	0.03	204	0.01
228	0.03	214	0.01
306	0.03	250	0.01
276	0.03	240	0.01
272	0.03	234	0.01
244	0.02	220	0.01

820 Table S 21. The estimated nitrate branching ratio (BR_{RONO2}) of α-pinene and β-pinene derived RO_2
821 under different assumptions.

RO_2	BR_{RONO2} (%) using calculated ring-opening fraction[a]	BR_{RONO2} (%) based on the same $BR_{RONO2,β\text{-}OH}$ assumption[b]	BR_{RONO2} (%) based on the different $BR_{RONO2,β\text{-}OH}$ assumption[c]	BR_{RONO2} (%) from Peeters et al.[d]	RO_2	BR_{RONO2} (%)[e]
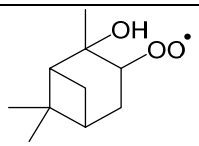 (2-OH,3-RO_2)	3.1	9.2	8.2	7	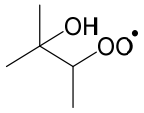	5.4
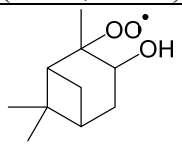 (3-OH,2-RO_2)	0.7	9.2	10.2	3	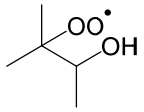	11
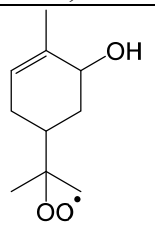 (3-OH,8-RO_2)	10.8	2.2	2.3	11		
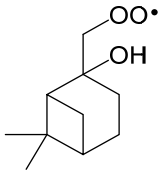 (2-OH,1-RO_2)	15.9	9.2	6.1		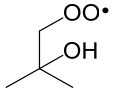	4.9
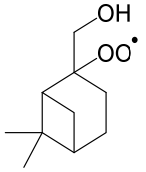 (1-OH,2-RO_2)	10.2	9.2	10.2		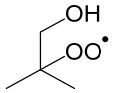	10
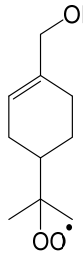 (1-OH,8-RO_2)	1.7	2.2	2.3			

822

[a]Assuming that BR_{add_C3} = 0.5, $BR_{\alpha\text{-pinene,ring-open}}$ = 0.32, BR_{add_C1} = 0.93, and $BR_{\beta\text{-pinene,ring-open}}$ = 0.44.

[b]Assuming that (1) the ring-opened RO_2 of both α-pinene and β-pinene have the same BR_{RONO2} and (2) all the β-hydroxy RO_2 have the same BR_{RONO2}. See section S6 for details.

[c]Assuming that (1) the ring-opened RO_2 of both α-pinene and β-pinene have the same BR_{RONO2} and (2) the ratio of BR_{RONO2} for tertiary, secondary, and primary β-hydroxy RO_2 is 1.25: 1: 0.75. See section S6 for details.

[d]Peeters et al.[56] estimated based on structure-activity-relationship.

[e]The BR_{RONO2} of 2-methyl 2-butene and methylpropene RO_2, which share a similar structure but different size as the substitutions on α-pinene and β-pinene C-C double bond, respectively. The values are experimentally constrained by Teng et al.[2]

References

1. Kurtén, T.; Møller, K. H.; Nguyen, T. B.; Schwantes, R. H.; Misztal, P. K.; Su, L.; Wennberg, P. O.; Fry, J. L.; Kjaergaard, H. G. Alkoxy Radical Bond Scissions Explain the Anomalously Low Secondary Organic Aerosol and Organonitrate Yields from A-Pinene + No3. *J. Phys. Chem. Lett* **2017**, 2826-2834.
2. Teng, A. P.; Crounse, J. D.; Lee, L.; St. Clair, J. M.; Cohen, R. C.; Wennberg, P. O. Hydroxy Nitrate Production in the Oh-Initiated Oxidation of Alkenes. *Atmos. Chem. Phys.* **2015,** *15*, 4297-4316.
3. O'Haver Interactive Peak Fitter. *Available at https://terpconnect.umd.edu/~toh/spectrum/InteractivePeakFitter.htm*. **2016**.
4. Saunders, S. M.; Jenkin, M. E.; Derwent, R. G.; Pilling, M. J. Protocol for the Development of the Master Chemical Mechanism, Mcm V3 (Part a): Tropospheric Degradation of Non-Aromatic Volatile Organic Compounds. *Atmos. Chem. Phys.* **2003,** *3*, 161-180.
5. Crounse, J. D.; Paulot, F.; Kjaergaard, H. G.; Wennberg, P. O. Peroxy Radical Isomerization in the Oxidation of Isoprene. *Phys. Chem. Chem. Phys.* **2011,** *13*, 13607-13613.
6. Teng, A. P.; Crounse, J. D.; Wennberg, P. O. Isoprene Peroxy Radical Dynamics. *J. Am. Chem. Soc.* **2017,** *139*, 5367-5377.
7. Garden, A. L.; Paulot, F.; Crounse, J. D.; Maxwell-Cameron, I. J.; Wennberg, P. O.; Kjaergaard, H. G. Calculation of Conformationally Weighted Dipole Moments Useful in Ion–Molecule Collision Rate Estimates. *Chem Phys Lett* **2009,** *474*, 45-50.
8. Paulot, F.; Crounse, J. D.; Kjaergaard, H. G.; Kroll, J. H.; Seinfeld, J. H.; Wennberg, P. O. Isoprene Photooxidation: New Insights into the Production of Acids and Organic Nitrates. *Atmos. Chem. Phys.* **2009,** *9*, 1479-1501.
9. Crounse, J. D.; Paulot, F.; Kjaergaard, H. G.; Wennberg, P. O. Peroxy Radical Isomerization in the Oxidation of Isoprene. *Phys Chem Chem Phys* **2011,** *13*, 13607-13613.
10. Werner, H.-J.; Knizia, G.; Manby, F. R. Explicitly Correlated Coupled Cluster Methods with Pair-Specific Geminals. *Molecular Physics* **2011,** *109*, 407-417.
11. Halgren, T. A. Mmff Vii. Characterization of Mmff94, Mmff94s, and Other Widely Available Force Fields for Conformational Energies and for Intermolecular-Interaction Energies and Geometries. *Journal of Computational Chemistry* **1999,** *20*, 730-748.
12. Halgren, T. A. Merck Molecular Force Field. V. Extension of Mmff94 Using Experimental Data, Additional Computational Data, and Empirical Rules. *Journal of Computational Chemistry* **1996,** *17*, 616-641.
13. Halgren, T. A.; Nachbar, R. B. Merck Molecular Force Field. Iv. Conformational Energies and Geometries for Mmff94. *Journal of Computational Chemistry* **1996,** *17*, 587-615.
14. Halgren, T. A. Merck Molecular Force Field. Iii. Molecular Geometries and Vibrational Frequencies for Mmff94. *Journal of Computational Chemistry* **1996,** *17*, 553-586.
15. Halgren, T. A. Merck Molecular Force Field. Ii. Mmff94 Van Der Waals and Electrostatic Parameters for Intermolecular Interactions. *Journal of Computational Chemistry* **1996,** *17*, 520-552.
16. Halgren, T. A. Merck Molecular Force Field. I. Basis, Form, Scope, Parameterization, and Performance of Mmff94. *Journal of Computational Chemistry* **1996,** *17*, 490-519.
17. Frisch, M. J.; Trucks, G. W.; Schlegel, H. B.; Scuseria, G. E.; Robb, M. A.; Cheeseman, J. R.; Scalmani, G.; Barone, V.; Petersson, G. A.; Nakatsuji, H., et al. *Gaussian 16 Rev. A.03*, Wallingford, CT, 2016.

18. Becke, A. D. Density-Functional Thermochemistry. Iii. The Role of Exact Exchange. *The Journal of Chemical Physics* **1993,** *98*, 5648-5652.
19. Lee, C.; Yang, W.; Parr, R. G. Development of the Colle-Salvetti Correlation-Energy Formula into a Functional of the Electron Density. *Physical Review B* **1988,** *37*, 785-789.
20. Hehre, W. J.; Ditchfield, R.; Pople, J. A. Self—Consistent Molecular Orbital Methods. Xii. Further Extensions of Gaussian—Type Basis Sets for Use in Molecular Orbital Studies of Organic Molecules. *The Journal of Chemical Physics* **1972,** *56*, 2257-2261.
21. Clark, T.; Chandrasekhar, J.; Spitznagel, G. W.; Schleyer, P. V. R. Efficient Diffuse Function-Augmented Basis Sets for Anion Calculations. Iii. The 3-21+G Basis Set for First-Row Elements, Li–F. *Journal of Computational Chemistry* **1983,** *4*, 294-301.
22. Frisch, M. J.; Pople, J. A.; Binkley, J. S. Self-Consistent Molecular Orbital Methods 25. Supplementary Functions for Gaussian Basis Sets. *The Journal of Chemical Physics* **1984,** *80*, 3265-3269.
23. Dunning Jr., T. H. Gaussian Basis Sets for Use in Correlated Molecular Calculations. I. The Atoms Boron through Neon and Hydrogen. *The Journal of Chemical Physics* **1989,** *90*, 1007-1023.
24. Møller, K. H.; Otkjær, R. V.; Hyttinen, N.; Kurtén, T.; Kjaergaard, H. G. Cost-Effective Implementation of Multiconformer Transition State Theory for Peroxy Radical Hydrogen Shift Reactions. *J. Phys. Chem. A* **2016,** *120*, 10072-10087.
25. *Spartan'16*, Wavefunction, Inc., Irvine, CA.
26. Chai, J.-D.; Head-Gordon, M. Long-Range Corrected Hybrid Density Functionals with Damped Atom-Atom Dispersion Corrections. *Physical Chemistry Chemical Physics* **2008,** *10*, 6615-6620.
27. Kendall, R. A.; Dunning Jr., T. H.; Harrison, R. J. Electron Affinities of the First-Row Atoms Revisited. Systematic Basis Sets and Wave Functions. *The Journal of Chemical Physics* **1992,** *96*, 6796-6806.
28. Adler, T. B.; Knizia, G.; Werner, H.-J. A Simple and Efficient Ccsd(T)-F12 Approximation. *Accounts of Chemical Research* **2007,** *127*, 221106.
29. Knizia, G.; Adler, T. B.; Werner, H.-J. Simplified Ccsd(T)-F12 Methods: Theory and Benchmarks. *The Journal of Chemical Physics* **2009,** *130*, 054104.
30. Peterson, K. A.; Adler, T. B.; Werner, H.-J. Systematically Convergent Basis Sets for Explicitly Correlated Wavefunctions: The Atoms H, He, B–Ne, and Al–Ar. *The Journal of Chemical Physics* **2008,** *128*, 084102.
31. Watts, J. D.; Gauss, J.; Bartlett, R. J. Coupled-Cluster Methods with Noniterative Triple Excitations for Restricted Open-Shell Hartree–Fock and Other General Single Determinant Reference Functions. Energies and Analytical Gradients. *The Journal of Chemical Physics* **1993,** *98*, 8718-8733.
32. Werner, H.-J.; Knizia, G.; R. Manby, F. Explicitly Correlated Coupled Cluster Methods with Pair-Specific Geminals. *Molecular Physics* **2011,** *109*, 407-417.
33. Werner, H.-J.; Knowles, P. J.; Knizia, G.; Manby, F. R.; Schütz, M. Molpro: A General-Purpose Quantum Chemistry Program Package. *Wiley Interdisciplinary Reviews: Computational Molecular Science* **2012,** *2*, 242-253.
34. Werner, H.-J.; Knowles, P. J.; Knizia, G.; Manby, F. R.; Schütz, M.; Celani, P.; Györffy, W.; Kats, D.; Korona, T.; Lindh, R., et al. *Molpro, Version 2012.1, a Package of Ab Initio Programs*, 2012.

35. Rienstra-Kiracofe, J. C.; Allen, W. D.; Schaefer, H. F. The C2h5 + O2 Reaction Mechanism: High-Level Ab Initio Characterizations. *The Journal of Physical Chemistry A* **2000,** *104*, 9823-9840.
36. Lambert, N.; Kaltsoyannis, N.; Price, S. D.; Žabka, J.; Herman, Z. Bond-Forming Reactions of Dications with Molecules: A Computational and Experimental Study of the Mechanisms for the Formation of Hcf2+ from Cf32+ and H2. *The Journal of Physical Chemistry A* **2006,** *110*, 2898-2905.
37. Jayatilaka, D.; Lee, T. J. Open-Shell Coupled-Cluster Theory. *The Journal of Chemical Physics* **1993,** *98*, 9734-9747.
38. Matlab R2016b.
39. Eckart, C. The Penetration of a Potential Barrier by Electrons. *Physical Review* **1930,** *35*, 1303-1309.
40. Evans, M. G.; Polanyi, M. Some Applications of the Transition State Method to the Calculation of Reaction Velocities, Especially in Solution. *Transactions of the Faraday Society* **1935,** *31*, 875-894.
41. Eyring, H. The Activated Complex and the Absolute Rate of Chemical Reactions. *Chemical Reviews* **1935,** *17*, 65-77.
42. Vereecken, L.; Peeters, J. The 1,5-H-Shift in 1-Butoxy: A Case Study in the Rigorous Implementation of Transition State Theory for a Multirotamer System. *The Journal of Chemical Physics* **2003,** *119*, 5159-5170.
43. Berndt, T.; Richters, S.; Jokinen, T.; Hyttinen, N.; Kurtén, T.; Otkjær, R. V.; Kjaergaard, H. G.; Stratmann, F.; Herrmann, H.; Sipilä, M., et al. Hydroxyl Radical-Induced Formation of Highly Oxidized Organic Compounds. *Nat. Commun.* **2016,** *7*, 13677.
44. Kurtén, T.; Møller, K. H.; Nguyen, T. B.; Schwantes, R. H.; Misztal, P. K.; Su, L.; Wennberg, P. O.; Fry, J. L.; Kjaergaard, H. G. Alkoxy Radical Bond Scissions Explain the Anomalously Low Secondary Organic Aerosol and Organonitrate Yields from A-Pinene + No3. *The Journal of Physical Chemistry Letters* **2017,** *8*, 2826-2834.
45. Glowacki, D. R.; Liang, C.-H.; Morley, C.; Pilling, M. J.; Robertson, S. H. Mesmer: An Open-Source Master Equation Solver for Multi-Energy Well Reactions. *J. Phys. Chem. A* **2012,** *116*, 9545-9560.
46. Chuong, B.; Davis, M.; Edwards, M.; Stevens, P. S. Measurements of the Kinetics of the Oh + A-Pinene and Oh + B-Pinene Reactions at Low Pressure. *International Journal of Chemical Kinetics* **2002,** *34*, 300-308.
47. Wu, D.; Bayes, K. D. Rate Constants for the Reactions of Isobutyl, Neopentyl, Cyclopentyl, and Cyclohexyl Radicals with Molecular Oxygen. *International Journal of Chemical Kinetics* **1986,** *18*, 547-554.
48. Allen, H. M.; Crounse, J. D.; Bates, K. H.; Teng, A. P.; Krawiec-Thayer, M. P.; Rivera-Rios, J. C.; Keutsch, F. N.; St. Clair, J. M.; Hanisco, T. F.; Møller, K. H., et al. Kinetics and Product Yields of the Oh Initiated Oxidation of Hydroxymethyl Hydroperoxide. *The Journal of Physical Chemistry A* **2018,** *122*, 6292-6302.
49. Forst, W. Analytic Solution of Relaxation in a System with Exponential Transition Probabilities. Iii. Macroscopic Disequilibrium. *The Journal of Chemical Physics* **1984,** *80*, 2504-2513.
50. Kurtén, T.; Rissanen, M. P.; Mackeprang, K.; Thornton, J. A.; Hyttinen, N.; Jørgensen, S.; Ehn, M.; Kjaergaard, H. G. Computational Study of Hydrogen Shifts and Ring-Opening

970 Mechanisms in A-Pinene Ozonolysis Products. *The Journal of Physical Chemistry A* **2015,** *119*,
971 11366-11375.
972 51. Cuadros, F.; Cachadiña, I.; Ahumada, W. Determination of Lennard-Jones Interaction
973 Parameters Using a New Procedure. *Molecular Engineering* **1996,** *6*, 319-325.
974 52. Su, T.; Chesnavich, W. J. Parametrization of the Ion–Polar Molecule Collision Rate
975 Constant by Trajectory Calculations. *The Journal of Chemical Physics* **1982,** *76*, 5183-5185.
976 53. Atkinson, R.; Aschmann, S. M.; Carter, W. P. L.; Winer, A. M.; Pitts, J. N. Alkyl Nitrate
977 Formation from the Nitrogen Oxide (Nox)-Air Photooxidations of C2-C8 N-Alkanes. *The Journal*
978 *of Physical Chemistry* **1982,** *86*, 4563-4569.
979 54. Eddingsaas, N. C.; Loza, C. L.; Yee, L. D.; Chan, M.; Schilling, K. A.; Chhabra, P. S.;
980 Seinfeld, J. H.; Wennberg, P. O. A-Pinene Photooxidation under Controlled Chemical Conditions
981 &Ndash; Part 2: Soa Yield and Composition in Low- and High-Nox Environments. *Atmos. Chem.*
982 *Phys.* **2012,** *12*, 7413-7427.
983 55. Bean, J. K.; Hildebrandt Ruiz, L. Gas–Particle Partitioning and Hydrolysis of Organic
984 Nitrates Formed from the Oxidation of A-Pinene in Environmental Chamber Experiments. *Atmos.*
985 *Chem. Phys.* **2016,** *16*, 2175-2184.
986 56. Nozière, B.; Barnes, I.; Becker, K.-H. Product Study and Mechanisms of the Reactions of
987 A-Pinene and of Pinonaldehyde with Oh Radicals. *Journal of Geophysical Research: Atmospheres*
988 **1999,** *104*, 23645-23656.
989 57. Cleaves, H. J., Branching Ratio. In *Encyclopedia of Astrobiology*, Gargaud, M.; Amils, R.;
990 Quintanilla, J. C.; Cleaves, H. J.; Irvine, W. M.; Pinti, D. L.; Viso, M., Eds. Springer Berlin
991 Heidelberg: Berlin, Heidelberg, 2011; pp 218-218.
992 58. Peeters, J.; Vereecken, L.; Fantechi, G. The Detailed Mechanism of the Oh-Initiated
993 Atmospheric Oxidation of A-Pinene: A Theoretical Study. *Phys. Chem. Chem. Phys.* **2001,** *3*,
994 5489-5504.
995 59. Vereecken, L.; Peeters, J. Theoretical Study of the Formation of Acetone in the Oh-
996 Initiated Atmospheric Oxidation of A-Pinene. *J. Phys. Chem. A* **2000,** *104*, 11140-11146.
997 60. Wennberg, P. O.; Bates, K. H.; Crounse, J. D.; Dodson, L. G.; McVay, R. C.; Mertens, L.
998 A.; Nguyen, T. B.; Praske, E.; Schwantes, R. H.; Smarte, M. D., et al. Gas-Phase Reactions of
999 Isoprene and Its Major Oxidation Products. *Chem. Rev.* **2018,** *118*, 3337-3390.
1000 61. Vereecken, L.; Muller, J. F.; Peeters, J. Low-Volatility Poly-Oxygenates in the Oh-Initiated
1001 Atmospheric Oxidation of A-Pinene: Impact of Non-Traditional Peroxyl Radical Chemistry. *Phys.*
1002 *Chem. Chem. Phys.* **2007,** *9*, 5241-5248.
1003 62. Aschmann, S. M.; Atkinson, R.; Arey, J. Products of Reaction of Oh Radicals with A-
1004 Pinene. *J. Geophys. Res. - Atmos* **2002,** *107*, ACH 6-1-ACH 6-7.
1005 63. Wisthaler, A.; Jensen, N. R.; Winterhalter, R.; Lindinger, W.; Hjorth, J. Measurements of
1006 Acetone and Other Gas Phase Product Yields from the Oh-Initiated Oxidation of Terpenes by
1007 Proton-Transfer-Reaction Mass Spectrometry (Ptr-Ms). *Atmospheric Environ.* **2001,** *35*, 6181-
1008 6191.
1009